REVIEW

Check for updates

Recent advances on the thermal destabilization of Mg-based hydrogen storage materials

Jianfeng Zhang, [ID] Zhinian Li,* Yuanfang Wu, Xiumei Guo, Jianhua Ye, Baolong Yuan, Shumao Wang and Lijun Jiang

Magnesium hydride and its compounds have a high hydrogen storage capacity and are inexpensive, and thus have been considered as one of the most promising hydrogen storage materials for on-board applications. Nevertheless, Mg/MgH$_2$ systems suffer from great drawbacks in terms of kinetics and thermodynamics for hydrogen uptake/release. Over the past decades, although significant progress has been achieved with respect to hydrogen sorption kinetics in Mg/MgH$_2$ systems, their high thermal stability remains the main drawback, which hinders their practical applications. Accordingly, herein, we present a brief summary of the synthetic routes and a comprehensive overview of the advantages and disadvantages of the promising strategies to effectively tune the thermodynamics of Mg-based materials, such as alloying, nanostructuring, metastable phase formation, changing reaction pathway, and nano Mg-based composites. Among them nanostructuring and metastable phase formation, which have the superiority of changing the thermodynamics without affecting the hydrogen capacity, have attracted increasing interest in this field. To further optimize the hydrogen storage performance, we specially emphasize novel nanostructured materials, which have the advantage of combining alloy engineering, nanostructuring and the synergistic effect to change the thermodynamics of Mg/MgH$_2$ to some extent. Furthermore, the remaining challenges and the directions of further research on MgH$_2$, including the fundamental mechanism of the Mg–H bond instability, advanced synthetic routes, stabilizing nanostructures, and predicting novel composite materials, are proposed.

1. Introduction

Energy is the basic requirement for human productivity and social activities. Recently, the consumption of fossil energy has remarkably increased with the development of the economy. Especially, after the eighteenth century industrial revolution, the consumption of fossil fuels such as coal, oil, and natural gas has increased dramatically in society. However, the problems of environmental pollution and exhaustion of energy resources caused by the over-use of fossil fuels have made it necessary to search for alternative energy carriers. Hydrogen is an energy carrier, which holds tremendous promise as a new clean energy option. Upon its conversion into energy using a fuel cell, only water is produced without any harmful emissions. Therefore, many countries have focused on the development and utilization of hydrogen energy a key research area. The research on good performance and high capacity hydrogen storage materials plays a crucial role in the large-scale applications and the realization of a "hydrogen economy". Hydrogen storage sectors can be classified into three broad categories, namely, a high-pressured gaseous state, a cryogenic liquid state, and a solid

state. However, currently, the storage of hydrogen gas in gas cylinders under high pressure is not safe. Similarly to pressurized hydrogen gas, liquid hydrogen possesses many difficulties related to its very low density and is not economic since a large amount of energy is consumed to cool the gas temperature to 20.2 K. Apart from the gaseous and liquid states for hydrogen storage, solid-state hydrogen storage systems have been considered as the most reliable and safe practical solution for providing clean energy for different applications at a desired temperature with low cost and high hydrogen capacity,[1] such as proton-exchange fuel cells membranes (PEM).[2]

In the 1960s, scientists in Holland found that the SmCo$_5$ magnetic alloy can absorb a large amount of hydrogen. Based on this, the LaNi$_5$-type hydrogen storage alloy was developed with a reversible hydrogen storage capacity of 1.4 wt% with a formation enthalpy of -30.2 kJ mol^{-1} at ambient temperature.[3] Around the same period, J. J. Reilly, a researcher at the Brookhaven National Laboratory in the United States, discovered the Mg$_2$Ni hydrogen storage alloy, with a reversible hydrogen storage capacity of 3.6 wt%.[4] In metal hydrides, the hydrogen atoms are chemically bonded with metallic elements such as intermetallic hydrides, complex hydrides, and elemental hydrides, where around 36 metallic elements can interrelate with hydrogen atoms. These metal hydrides, such as LaNi$_5$, TiFe, and V-based solid solution, have suitable hydrogen sorption

General Research Institute for Nonferrous Metals, 2 Xinjiekou Wai Street, Beijing 100088, China. E-mail: lzngrinm@163.com; Fax: +86-10-60662619; Tel: +86-10-60662633

thermodynamics and fast kinetics, which mean that hydrogen sorption can take place at a fast rate and suitable temperatures and hydrogen pressure conditions. Unfortunately, they all have a very low gravimetric hydrogen storage density (Fig. 1)[5] and are unsuitable for practical application as energy sources, particularly as on-board automotive hydrogen storage systems according to the US-Department of Energy (DOE) (Table 1).[6]

From Fig. 1, Mg-based hydrides can be considered as an efficient on-board hydrogen storage candidate especially for vehicular application due to their high hydrogen content of 7.6 wt% and volumetric density of about twice that of liquid hydrogen (consistent with the goals of the DOE). http://www.youdao.com/w/eng/destabilized/javascript:void(0); The use of Mg for hydrogen storage purposes also has other potential advantages. Mg is the 8th most abundant element in the Earth's crust (2.3%) and the 3rd most abundant element dissolved in sea water. Thus, Mg-based storage materials have the potential of low cost and are considered to be the most promising hydrogen storage materials for light-duty vehicles. However, a number of issues need to be solved before their practical application, such as high desorption temperature, kinetic limitations of Mg/MgH_2, and easy oxidation in oxygen and air. In the past few decades, significant progress has been made in improving the hydrogenation/dehydrogenation kinetics of Mg-based materials by adding a catalyst, multiphase composite, nanocrystalline and other measures. However, the tuning of their thermodynamic properties is still a great challenge. Herein, we present a summary on the recent advances and developments of Mg and Mg-based materials.

2. Magnesium hydride as hydrogen storage medium

The crystal structure of pure magnesium is close-packed hexagonal and it can react with hydrogen at the temperature
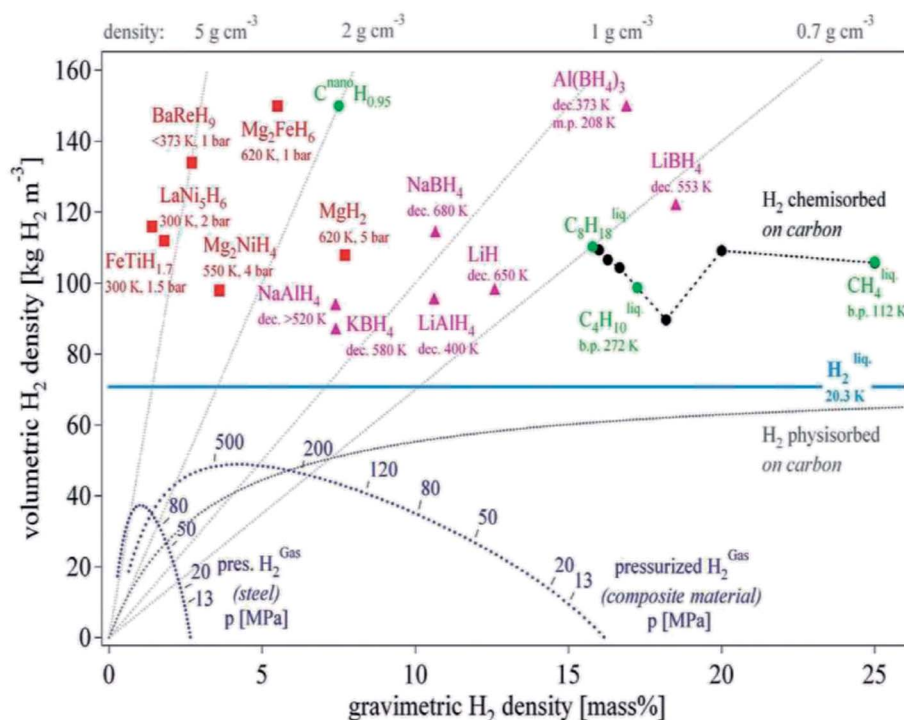

Fig. 1 Gravimetric and volumetric hydrogen density of various hydrogen storage materials.[5]

Table 1 Main technical targets for onboard hydrogen storage systems for light-duty fuel cell vehicles by the US DOE[6]

Parameters	Units	Year 2020	Year 2025	Ultimate	Related properties of materials
System gravimetric capacity	kW h kg system	1.5	1.8	2.2	Storage capacity
	kg H_2/kg system	0.045	0.055	0.065	
System volumetric capacity	kW h L system	1.0	1.3	1.7	Storage capacity
	kg H_2/L system	0.030	0.040	0.050	
Min/max delivery temperature	°C	40/85	40/85	40/85	Kinetics, thermodynamics
System fill time	Min	3–5	3–5	3–5	Kinetics
Operational cycle life (1/4 tank to full)	Cycles	1500	1500	1500	Cycle ability
Fuel cost	USD/kW h	10	9	8	Storage capacity
	Net (USD/kg H_2)	(333)	(300)	(266)	Composition

Table 2 Crystal structure data for Mg, γ-MgH₂ and β-MgH₂ (ref. 11)

Component phase	Crystal structure	Unit cell parameters (Å)	ΔH (kJ mol⁻¹ H₂)/110 surface energy of plane[12] (J m²)	ΔH (kJ mol⁻¹ H₂)/001 surface energy of plane[12] (J m²)
Mg	Hexagonal	$a = 3.2094$, $c = 5.2112$, $V = 46.48$ Å³		
α-MgH₂	Tetragonal	$a = 4.5010$, $c = 3.0100$		
β-MgH₂	Hexagonal	$a = 4.5180$, $c = 3.0205$, $V = 61.63$ Å³	78.16/0.19	50.75/1.09
γ-MgH₂	Orthorhombic	$a = 4.5300$, $b = 5.4400$, $c = 4.9300$, $V = 121.49$ Å³	44.66/1.23	54.41/0.97

of 573–673 K and 2.4–40 bar hydrogen pressure, which involves a number of different steps, such as physisorption, dissociation, chemisorption, diffusion of hydrogen into its subsurface sites and bulk lattice sites and finally the nucleation and growth of the hydride phase. Upon the application of hydrogen pressure to Mg, the hydrogen atoms initially occupy the tetrahedral interstitial sites within its lattice, forming a tetragonal α-phase with a hydrogen concentration of up to 0.4 wt%.[7] At higher pressures, the nucleation of the β-phase is energetically favorable and the α-phase is converted into hexagonal structure β-MgH₂. During this process, the hexagonal close-packed (hcp) lattice of Mg expands by approximately 30% (Table 2), and this phase further transitions to the metastable γ-MgH₂ phase under higher compressive stress (70–80 bar).[8–10] Recently, researchers discovered that the coexistence of different types MgH₂ can produce a catalytic effect during hydrogen release/uptake, for example, γ-MgH₂ will make β-MgH₂ destabilize to release hydrogen at low temperature. Unfortunately, γ-MgH₂ will irreversibly revert to β-MgH₂ upon the first hydrogen cycle at 573 K.[10]

Magnesium hydride differs to other metal hydrides in its M–H bonds and crystal structure, which is similar to ionic hydrides of alkali and alkaline earth metals. Vajeeston *et al.* revealed that all polymorphs of MgH₂ have a dominant ionic character with Mg and H in nearly 2⁺ and 1⁻ states, respectively, by means of charge-density, charge-transfer, electron-localization function and Mulliken population analyses.[11] The strong chemical bonds formed between hydrogen and metals during chemisorption explain the high storage capacity of Mg and its stability at room temperature. Thereby, the reaction of hydrogen with Mg is exothermic with an enthalpy of reaction of -74.5 kJ (mol⁻¹ H₂) and an entropy variation of -135 J (K⁻¹ mol⁻¹ H₂), which is much larger than the practical requirements for metal hydrides of 20–40 kJ mol⁻¹ and results in a higher desorption temperature.[13] Fig. 2 shows the variation in the plateau pressure as a function of temperature for MgH₂. Accordingly, it can be concluded that magnesium cannot absorb hydrogen below a pressure of 10 bar if the temperature is higher than about 640 K. Similarly, magnesium hydride has to be heated to at least 550 K to desorb hydrogen under 1 bar of pressure. Thus, the challenge is to reduce the operation temperature while retaining as much as possible its high hydrogen storage capacity.[14]

3. Preparation of MgH₂

The reaction of Mg with hydrogen yields a stable hydride as follows (1):

$$Mg + H_2 \leftrightarrow MgH_2 \tag{1}$$

Thus far, many techniques have been developed to synthesize MgH₂ for hydrogen storage, such as mechanical milling,[15] thin film technology,[16] hydrogen plasma metal reaction,[17] hydriding chemical vapor deposition,[18] melt spinning,[19] severe plastic deformation,[20] chemical reduction,[21] and electrochemical deposition.[22] One of the most commonly used techniques is reactive mechanical milling (RMM), which has been widely used to tune metal microstructures to modify their hydrogenation properties.[23] Its advantages as an efficient tool for the synthesis of hydrogen storage materials include the ease of hydrogenation of Mg-based alloys at low temperature, the generation of fresh and highly reactive surfaces, the ease of formation of multi-phase nanocomposites and creation of more defects and micro-strains in the crystal lattice due to mechanical action.[24] As shown in Fig. 3, the desorption plateau of the milled sample is much higher and the hysteresis much smaller,
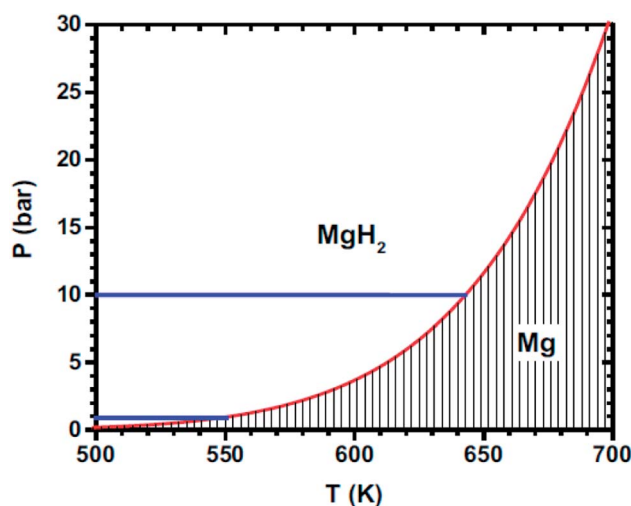

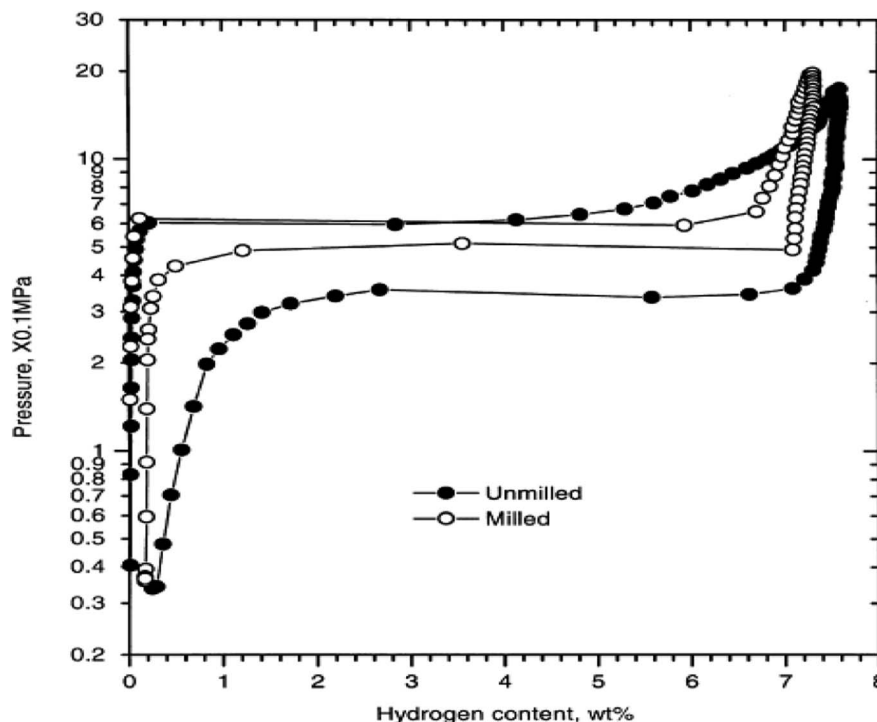**Fig. 2** Temperature dependence of the dissociation pressure of MgH₂.[14]

Fig. 3   Pressure–composition–temperature (PCT) curves of the unmilled and ball-milled MgH$_2$ at 623 K.[25]

indicating very fast desorption kinetics due to the novel nano-structures with a high surface area caused by ball milling (BM).[25]

Currently, the mechanochemical synthesis of metal hydrides using RMM has become one of the most frequently used methods. Generally, mill machines can be classified into four categories: planetary, rotational, vibratory and attritor mills.[15] Considering the final products expected from BM, several milling parameters can be varied in the ball-milling synthesis, including the type of milling bowl and ball, milling speed, milling time, ball-to-powder weight ratio, milling atmosphere,

pressure of the selected gas, temperature of milling, and process control agents to inhibit particle agglomeration. Varin et al.[26] investigated the effect of ball milling time on the particle and grain/crystallite size and clearly showed that a particle size reduction occurs within a very similar time frame as the reduction in grain size (Fig. 4). Besides Jain et al.[23] systematically investigated the role of ball milling in improving the surface and kinetic properties in the preparation of Mg-based alloys. They concluded that the pulverization and deformation processes during high energy ball milling play a major role in the hydriding reaction. Thus far, RMM under hydrogen gas
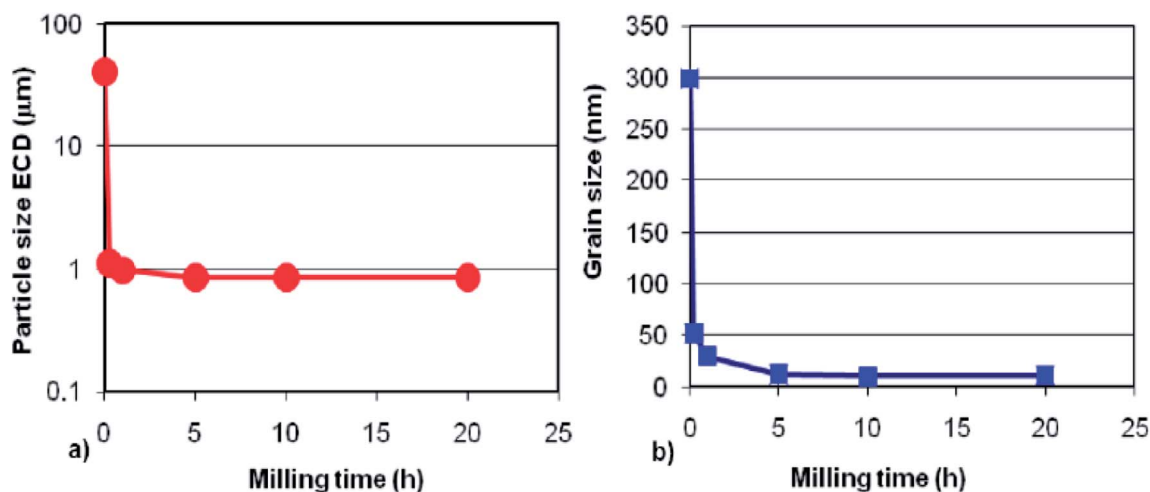

Fig. 4   Simultaneous reduction in the (a) particle size and (b) grain size as a function of ball milling time of MgH$_2$.[26]

allows the synthesis of binary and ternary metal hydrides (Mg–Fe–H, Mg–Co–H, Mg–Ni–H, Mg–Ti–H), Mg-based complex hydrides and alanates.[27] However, the preparation of such small particles by ball milling on a large scale is a major challenge.

4. Approaches to modify the thermodynamics of Mg/MgH₂ systems

As mentioned before, the stable thermodynamics of MgH_2 is the major obstacle in its practical application. According to the van't Hoff equation, we can conclude that changing the enthalpy and entropy of the hydrogenation reaction is an efficient way to decrease the desorption temperature of Mg/MgH_2 systems. Considering that changing the entropy has little effect on metal hydrogen systems, decreasing the enthalpy change for the reaction is the basic guideline for decreasing the desorption temperature of Mg/MgH_2 systems. In this section, we present the strategies for modifying the thermodynamics of MgH_2, such as alloying, nanostructuring, metastable phase formation and changing the reaction path.

4.1 Alloying

Generally, hydrogen storage alloys consist of a high temperature hydride forming element A and a non-hydride forming element B (Fig. 5).[28] If Mg-based alloys are made with a hydride non-forming element and form less stable hydrides to destabilize the hydrogenated state, the hydriding reaction enthalpy can be remarkably decreased. Therefore, alloying is a traditional but effective strategy for altering the thermodynamics of Mg-based alloys.

4.1.1 Intermetallic compounds. A classic example of alloying is the Mg_2NiH_4 compound, which was first reported by Reilly in 1968. Mg_2Ni is also a potential hydrogen storage material owing to its high hydrogen storage capacity of 3.6 wt%.[29,30] Since the Ni–H interaction in Mg_2NiH_4 is much

weaker than that in pure MgH_2, Mg_2NiH_4 has an enthalpy of formation of around -64 kJ mol^{-1} H$_2$, which means that its desorption temperature is around 523 K with a plateau pressure of around 3.4 bar at room temperature. Mg_2Ni was further studied by applying the element substitution method to further decrease its enthalpy of hydrogen absorption and desorption. Hou *et al.* reported an improvement in the enthalpy of formation of Mg_2Ni-type alloys by introducing a fraction of Zn or Ti in place of Mg, such as $Mg_{1.875}Zn_{0.125}NiH_4$ with an enthalpy of formation of -53.43 kJ mol^{-1} H$_2$.[31] Another interesting finding is that $(Mg_{1-x}Ca_x)Ni_2$-based alloys can desorb hydrogen at room temperature and the hydride formation enthalpy and entropy of $(Mg_{0.68}Ca_{0.32})Ni_2$ were determined to be $\Delta H = -37$ kJ (mol^{-1} H$_2$) and $\Delta S = -94$ J (K^{-1} mol^{-1} H$_2$), respectively. Unfortunately, with a decrease in its Mg content, its hydrogen storage capacity decreased to 1.4 wt%.[32]

Similarly to the Mg–Ni system, Mg and Cu can form the Mg_2Cu alloy. Upon the application of 30 MPa hydrogen pressure to Mg_2Cu, it decomposes to MgH_2 and $MgCu_2$ according to the following disproportionation reaction (2):

$$2Mg_2Cu + H_2 \rightarrow 3MgH_2 + MgCu_2 \qquad (2)$$
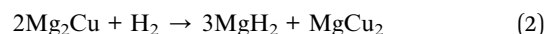
The hydride formation enthalpy and entropy of reaction (2) is -73.5 kJ (mol^{-1} H$_2$) and -146 J (K^{-1} mol^{-1} H$_2$), respectively, with a hydrogen capacity of 2.6 wt%,[33] and the equilibrium temperature for 1 bar hydrogen pressure is reduced to about 513 K. Unfortunately, this reaction is irreversible. Advanced research has shown that Mg–Cu–H nanoparticle systems can further reduce the hydride formation enthalpy and entropy to -67.5 kJ (mol^{-1} H$_2$) and -124.4 J (K^{-1} mol^{-1} H$_2$), respectively.[34] Thus from the above research, we can preliminarily conclude that nanostructuring of Mg-based alloys provides a potential strategy to further alter their thermodynamic properties without loss in their hydrogen capacity.

Normally, Mg and Fe are immiscible, but the ternary hydride Mg_2FeH_6 can be formed in the presence of hydrogen by mechanical milling. The hydride formation enthalpy and entropy are -77.9 kJ (mol^{-1} H$_2$) and -140 J (K^{-1} mol^{-1} H$_2$), respectively. Furthermore, it has a gravimetric storage capacity of 5.6 wt% and the highest known volumetric hydrogen density, amounting to 150 kg m^{-3}, which is more than double that of liquid hydrogen at 20.2 K and moderate pressures up to 20 bar.[35] The theoretical research conducted by Batalović[36] demonstrated the influence of transition metal (Ni, Co, and Mn) doping on the hydrogen sorption properties of Mg_2FeH_6. They found that the largest decrease in desorption enthalpy was in the case of nickel doping, resulting in a 27.7 kJ (mol^{-1} H) energy change. Similarly to the Mg–Fe system, reactive ball-milling of Mg and Co under hydrogen gas led to the formation of Mg_2CoH_5 with the gravimetric storage capacity of 4.5 wt%, hydride formation enthalpy of -82 kJ mol^{-1} H$_2$ and desorption temperature for 1 bar hydrogen pressure of about 513 K.[37] It is important to highlight that the formation of Mg_2FeH_6 consists of two steps that always involve MgH_2 as a precursor, which was also confirmed by the *in situ* hydrogen uptake curve (Fig. 6) monitored during the synthesis of Mg_2TM (TM = Fe and Co)
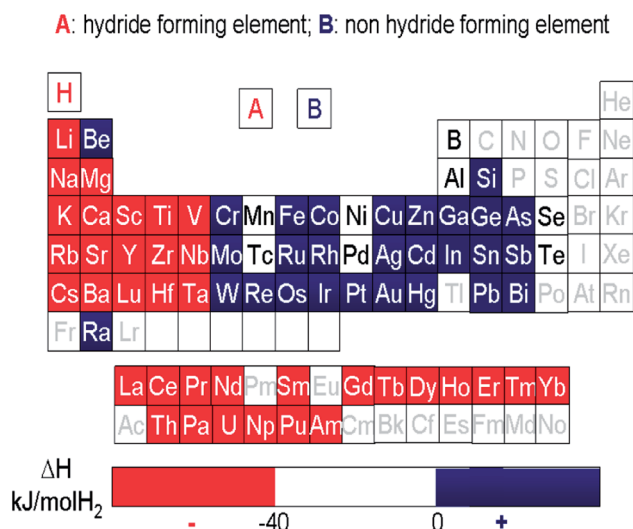

A: hydride forming element; **B**: non hydride forming element

Fig. 5 Hydride and non-hydride forming elements in the periodic table of elements.[28]
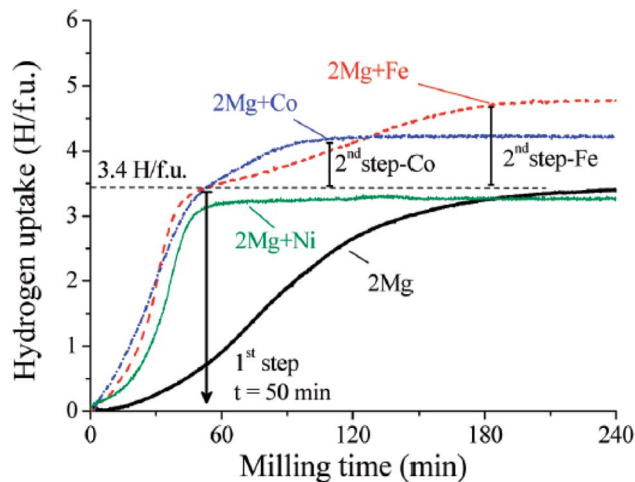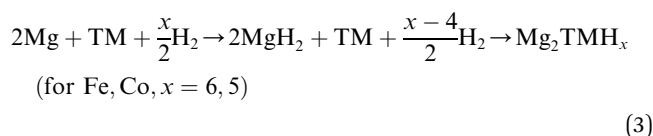
Fig. 6 Absorbed hydrogen atoms by formula unit of the formed hydride during RBM of Mg and Mg^{+2}TM mixtures (TM = Ni, Fe, and Co) (The number of absorbed H atoms per unit metal or alloy formula (H/f.u.)).[38]

Fig. 7 PCT diagrams of the studied Mg_3Cd alloy in the temperature range of 250–300 °C. The open and filled symbols correspond to the absorption and desorption branches of the curves, respectively.[42]

hydrides according to reaction (3);[38] whereas, a unique absorption step was detected in the case of Ni.[39]

$$2Mg + TM + \frac{x}{2}H_2 \rightarrow 2MgH_2 + TM + \frac{x-4}{2}H_2 \rightarrow Mg_2TMH_x$$
$$\text{(for Fe, Co, } x = 6, 5)$$

(3)

4.1.2 Mg-based solid solution. Forming an Mg-based solid solution is another destabilization strategy, which can apply a minor modulation to the structure and composition of Mg with an acceptable loss in capacity, thus probably altering its thermodynamic stability. Cadmium is the only element exhibiting unlimited solubility in Mg in the solid state. Douglass et al.[40] first reported the Mg-1 at% Cd alloy, which can absorb 5 wt% hydrogen at 673 K in 24 h. Schulz performed a more detailed study of the hydrogenation kinetics and thermodynamics of Mg-x at% Cd (x = 5, 10, and 20), which could be activated for hydrogen absorption even after annealing at 523 K for 24 h under the hydrogen pressure of 1.5 MPa.[41] However, Skripnyuk et al. prepared Mg_3Cd alloys using high energy milling, which exhibited a reversible hydrogen storage capacity of 2.8 wt% and could quickly absorb 2.5 wt% hydrogen at 573 K in 120 s. As shown in Fig. 7, no measurable pressure hysteresis was observed from the PCT, and the formation enthalpy of the hydride is -65.5 kJ mol^{-1}.[42]

According to the binary phase diagram of the Mg–In system, it has a high solubility of up to 10 at% indium in a wide temperature range.[43] The Mg (In) solid solution absorbs hydrogen to form MgH_2 and a disordered Mg–In compound. Table 3 summaries the lattice constants and hydrogen storage properties of Mg (In) solid solutions. The $Mg_{0.95}In_{0.05}$ solid solution can reversibly react with hydrogen at 573 K according to the following reaction (4):
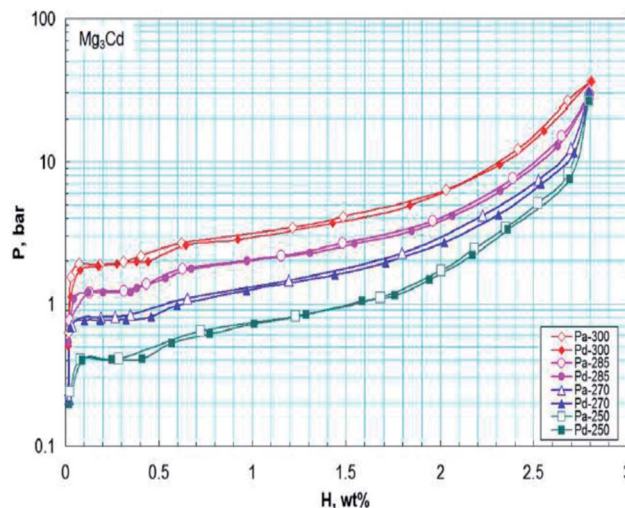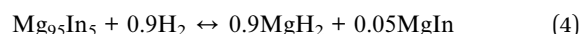
$$Mg_{95}In_5 + 0.9H_2 \leftrightarrow 0.9MgH_2 + 0.05MgIn$$

(4)

The hydrogen storage capacity of $Mg_{0.95}In_{0.05}$ is about 5.3 wt%, but the poor kinetics of its desorption/absorption reaction is a key problem.[44] Thus, Zhu et al. conducted research on Mg-based solid solutions, including Mg (In, Al), Mg (In, Cd) and Mg (In, Y) ternary alloys. Compared with the binary Mg (Al) solid solution, the Mg (In, Al) ternary solid solution presented improved dehydriding reversibility and a substantial decrease in ΔH because Al was dissolved in the β phase.[45]

With respect to the Mg–In–Y ternary system, the reversible dissolving of Y in Mg was realized by the decomposition of the In_3Y phase in dehydriding, but the reversible solubility of Y is rather low due to the formation of YH_2. The $Mg_{90}In_5Y_5$ solid solution exhibited a decreased reaction enthalpy of 62.9 kJ (mol^{-1} H_2), which was reduced by 5 kJ (mol^{-1} H_2) and 12 kJ (mol^{-1} H_2) compared to that of the $Mg_{95}In_5$ binary solid solution and pure Mg, respectively.[46] Similarly to the Mg–In–Y system, the hydriding reaction of the $Mg_{90}In_5Cd_5$ alloy can be described as reaction (5):

$$Mg_{90}In_5Cd_5 + 70H_2 \leftrightarrow 70MgH_2 + 5MgIn + 5Mg_3Cd$$

(5)

The dehydriding reaction enthalpy ΔH and entropy ΔS for the $Mg_{90}In_5Cd_5$ alloy are 86.0 kJ (mol^{-1} H_2) and 154.8 J (K^{-1} mol^{-1} H_2), respectively. The PCT results showed a reversible hydrogen storage capacity of 4.3 wt% and elevated equilibrium pressure for the MgH_2 in the $Mg_{90}In_5Cd_5$ alloy compared with pure MgH_2 (Fig. 8). The $Mg_{90}In_5Cd_5$ alloy also exhibited enhanced hydrogenation kinetics with a decreased hydrogenation activation energy of 61.0 kJ mol^{-1}, but its dehydrogenation rate is slow due to the long-range diffusion of In and Cd in MgH_2.[47] Mg-based solid solutions can reduce the reaction enthalpy with a higher hydrogen capacity than the Mg–Ni alloy

Table 3 Lattice constants of Mg-based solid solutions and their hydrogen storage properties[44]

Solid solution	Lattice constants (nm)		$|\Delta H|$ (kJ (mol^{-1} H$_2$))	ΔS (J (K^{-1} mol^{-1} H$_2$))	Capacity (wt%)
	a	c			
$Mg_{0.9}In_{0.1}$	0.31929	0.52061	65.2	121.8	4.2
$Mg_{0.95}In_{0.05}$	0.32027	0.52086	68.1	125.5	5.3
$Mg_{0.98}In_{0.02}$	0.32077	0.52106	69.6	126.0	6.4
$Mg_{0.75}Al_{0.25}$	0.31990	0.51960	76.8	138.6	5.0
$Mg_{0.9}In_{0.05}Al_{0.05}$	0.31980	0.51929	66.3	121.2	4.8
$Mg_{90}In_5Cd_5$	0.31925	0.51964	86	154.8	4.3
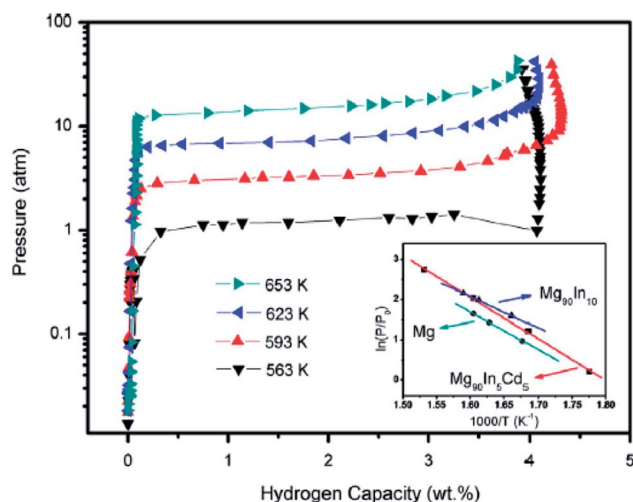
Fig. 8 PCT and van't Hoff plot (the inset) for the hydrogen desorption of the $Mg_{90}In_5Cd_5$ alloy.[47]

and even can compete with the Mg–Fe alloy in terms of hydrogen capacity, but their sluggish kinetics is still an issue.

Generally, alloying is a feasible way to modify the thermodynamics of Mg-base hydrogen storage alloys. However, there still exists some disadvantages, such as the hydrogen capacity decreases sharply after alloying due to the introduction of heavy metals and most of these Mg-base alloys still suffer from poor reversibility because the bonds between Mg and the other element break during the process of hydrogenation. Besides, Mg–Fe, Mg–Co, and Mg (In, Cd) present a higher ΔH for the dehydrogenation reaction than Mg/MgH$_2$; thus further research should be performed to address their remaining problems.

4.2 Nanostructuring

A major feature that discriminates various types of nanostructures is the dimensionality of their architecture, for example, zero-dimensional (0D; such as nanoparticles (NPs), quantum dots, and hollow spheres), one-dimensional (1D; such as nanowires, nanofibers, nanorods and nanobelts), two-dimensional (2D; such as thin films and nanosheets), and three-dimensional (3D; such as frameworks, nanoflowers, and dendritic structures), as demonstrated in Fig. 9.[48] Nanomaterials exhibit numerous advantages for batteries, fuel cells, and hydrogen storage systems. For example, with the

decreasing size of a material, its surface-to-volume ratio increases apparently. Moreover, the atoms on the surface may have some dangling bonds, which are extremely active and tend to form bonds with surrounding molecules to reduce the surface energy. Thus, reducing the particle and grain size of Mg-based materials is a promising way to further decrease their hydride formation enthalpy ΔH.

4.2.1 Nanoparticles or nanocrystalline material. For particles of sufficiently small size, the surface energy terms cannot be ignored. In the particular case of hydrogen desorption from MgH$_2$, the inclusion of these surface energy terms gives a new van't Hoff reaction (6) as follows:[49]

$$\ln \frac{p_{nano}^{eq}}{p^\theta} = \frac{1}{RT}\left[\Delta H^\theta + \left(\frac{3V_{Mg}\gamma_{Mg}}{r_{Mg}} - \frac{3V_{MgH_2}\gamma_{MgH_2}}{r_{MgH_2}}\right)\right] - \frac{\Delta S^\theta}{R}$$

(6)

Bulk MgH$_2$ is destabilised when the contribution related to size becomes sufficiently negative, *i.e.* the surface energy density of MgH$_2$ is significantly larger than that of magnesium, and some of the heat of formation will be stored as excess surface energy, which will reduce the heat released upon hydride formation and hydrogen release. Wagemans *et al.* predicted a considerable reduction (>10%) in ΔH for radii smaller than 4 nm, while DFT calculations predicted a result below 2 nm. The calculations showed that MgH$_2$ is more destabilized than Mg upon decreasing the cluster size below 19 Mg atoms (Fig. 10). For instance, an Mg$_9$H$_{18}$ cluster size of 0.9 nm corresponds to a desorption temperature of only 473 K with an enthalpy formation of −63 kJ mol^{-1} H$_2$.[50] Liu *et al.* successfully synthesized Mg nanoparticles by reducing di-*n*-butyl magnesium with lithium in the presence of naphthalene as an electron carrier. Further determination of the hydrogen thermodynamics of these materials revealed a significant evolution in both enthalpy and entropy with a decrease in particle sizes (Fig. 11). Hence, a ΔH of 63.5 ± 1.8 kJ (mol^{-1} H$_2$) and ΔS of 118.4 ± 3.1 J (K^{-1} mol^{-1} H$_2$) were measured for MgLi$_{4.6}$Napth$_{0.5}$ with an average particle size of 16 nm.[51]

Recently, there have been numerous methods reported for the preparation of MgH$_2$ NPs, including ball milling, hybrid combustion, melt spinning, and chemical vapour deposition (CVD). The nanostructured uniform mixture of MgH$_2$–0.1TiH$_2$ powder is a reversible hydrogen storage material with a cyclic hydrogen storage capacity of 6 wt%, which demonstrated good
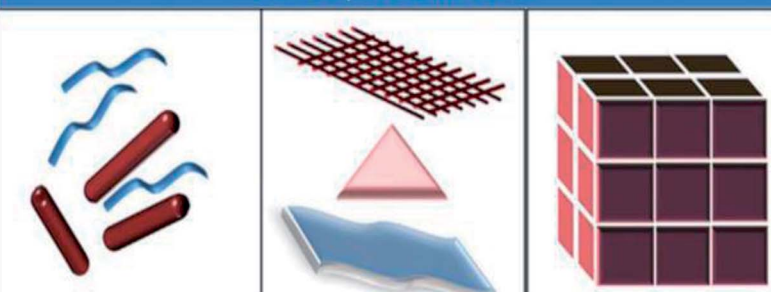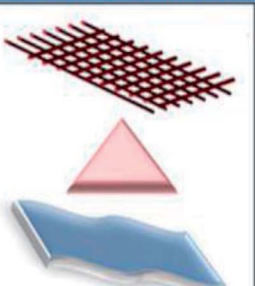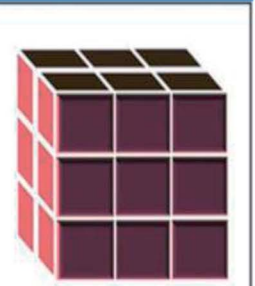
Fig. 9 Schematic representation of the various dimensions (0D, 1D, 2D, and 3D) of nanomaterials.[48]

cycling stability with no loss in capacity over 80 cycles. The ΔH for the dehydrogenation of MgH_2–0.1TiH_2 is 68 kJ $(mol^{-1}\ H_2)$, which is lower than that for MgH_2 (75 kJ $(mol^{-1}\ H_2)$). This can be attributed to two factors, its nanosize and the addition of TiH_2.[52] Besides, Asano et al.[53] demonstrated clearly that embedding Mg nanometer-sized clusters in a matrix of immiscible metals is a powerful strategy to destabilize MgH_2, resulting in a lower working temperature for hydrogen storage applications. Carbon-based materials also show huge potential in improving the hydrogen storage performance of MgH_2. Several works have been devoted to combining MgH_2 with various carbon materials, for example, nanocomposite (Mg–V)$_{nano}$/G exhibits a reversible hydrogen capacity of 6.03 wt% with an enthalpy of formation of -68.8 ± 2.3 kJ $(mol^{-1}\ H_2)$[54] and the magnesium particles with a carbon additive were milled to 20–60 nm with enthalpy and entropy changes of 44.5 kJ $(mol^{-1}\ H_2)$ and 83.8 J $(K^{-1}\ mol^{-1}\ H_2)$, respectively according to Fig. 12.[55] Graphite and carbon as a process control agent (PCA)

can reduce the agglomeration of the milled particles, and thus allow better particle refinement by stabilizing the surface charges created at the fresh surfaces of the fractured particles. In summary, it has been clearly demonstrated that the use of carbon materials offers many opportunities in tailoring the properties of metal hydrides. Since their porosity and surface chemistry can be adjusted in a broad range, their use as a support shows great potential for further improvements in hydrogen storage applications.

The formation of a nanocrystalline structure and associated defects through mechanical milling is often perceived as leading to enhanced hydrogen kinetics. Similarly to the case of surfaces discussed above, grain boundaries between nano-crystals contain excess energy, resulting in surface energy, thus providing another potential tool for reducing the formation enthalpy of metal hydrides. Calizzi et al.[56] prepared Mg–Ti nanostructured samples with a metastable Mg–Ti–H fcc phase and the mean crystallite size of Mg and β-MgH_2 decreased with an increase in Ti content (Fig. 13). However, their results only
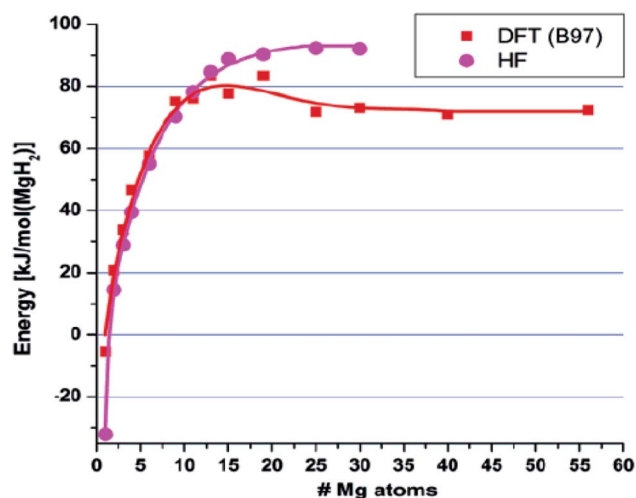

Fig. 10 Calculated desorption energies for MgH_2 clusters using both the HF method and DFT method (B97 functional). The energies were normalized per mole of H_2 released.[50]
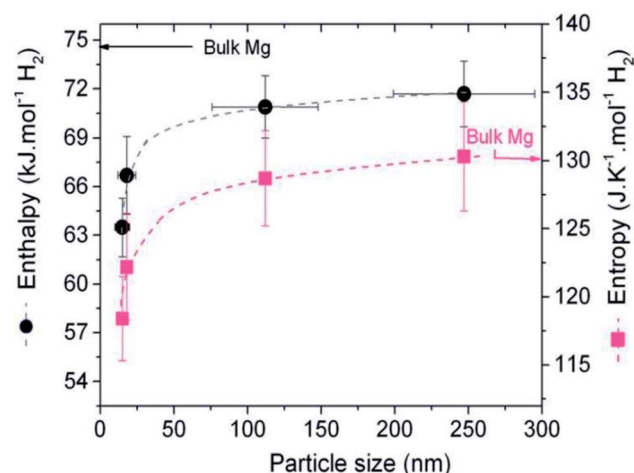

Fig. 11 Evolution of ΔH and ΔS versus size of the magnesium nano-particles. The dotted line is a guide to the eyes.[51]
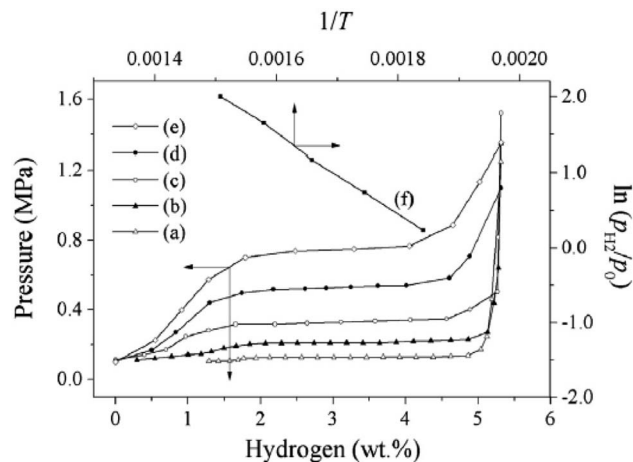
Fig. 12 Dehydrogenation isotherms of the material from Mg and C in a ratio of 70 : 30, milled for 3 h under 1 MPa H_2 at 543 K (a), 573 K (b), 603 K (c), 633 K (d), and 663 K (e), and plot of $\ln(P_{H_2}/P_0)$ versus $1/T$ (f).[55]

showed an enhanced kinetic properties in the Mg–Ti system since the modification in thermodynamics due to interface energy effects or coherency strain may be too small to be detected. Further research showed that the hydriding enthalpy of Mg–Fe-based materials with a crystallite size of 10 nm decrease by 6 kJ $(mol^{-1} H_2)$ between 523 K and 673 K (ref. 57) and an La_2Mg_{17}–$LaNi_5$ nanocrystalline composite material had a lower enthalpy of -53.23 kJ $(mol^{-1} H_2)$.[58]

Although the surface energy, lattice strain and defects, and excess enthalpy in the grain boundaries provide effective ways to lower the enthalpy of formation without loss in hydrogen storage capacity, they are usually unstable since the excess enthalpy will increase the free energy and drive recrystallization. Nanocrystalline MgH_2 resulting from ball milling undergoes a significant growth in crystallite size or subsequent structural relaxation of defects upon the very first hydrogen cycle, which sluggishly decreases the advantages of
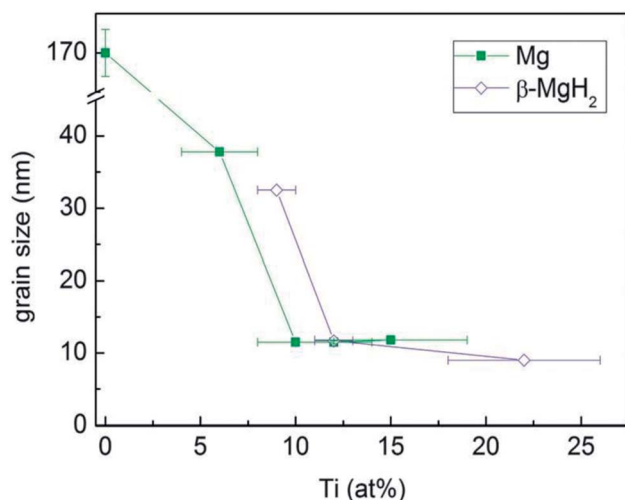

Fig. 13 Mean crystallite size of the Mg and β-MgH_2 phases in the Mg–Ti and Mg–Ti–H samples as a function of Ti content.[56]

nanocrystallization. Therefore, finding a proper way to protect NPs from aggregation or recrystallization is urgent.

4.2.2 Nanowires and nanofiber. Li et al.[59] prepared different Mg nanowires via a vapor-transport approach, with a diameter in the range of 30–50 nm (S1) (Fig. 14(a, b, g, h, and i)) and 80–100 nm (S2), which appeared to be tangled together and have a zigzag morphology (Fig. 14(c and d)), and short and rod-like structures of Mg with a diameter in the range of 150–170 nm (S3) (Fig. 14(e and f)). The calculated ΔH values for the dehydriding of the S1, S2, and S3 hydrides were 65.3, 65.9, and 67.2 kJ $(mol^{-1} H_2)$, respectively. It is apparent that the Mg nanowires with thinner diameters have the advantage of easy activation for hydrogen absorption/desorption (Fig. 14(j and k)). The presented results showed that thinner Mg/MgH_2 nanowires have a much lower desorption energy than that of thicker nanowires or bulk Mg/MgH_2, indicating that changes in thermodynamics are expected if the diameters of the nanowires are thinner than 30 nm.

They further studied the size effects on the thermodynamic stability of MgH_2 nanowires as well as the size dependency on the energetic stability of magnesium and MgH_2 nanowires using first-principles density functional theory.[60] The desorption enthalpy, ΔH_{des}, was calculated to be -20.64, 34.54, and 61.86 kJ $(mol^{-1} H_2)$ for the nanowires of A1_MgH_2 (φ0.68 nm), A2_MgH_2 (φ0.85 nm), and A3_MgH_2 (φ1.24 nm), as shown in Fig. 15. Thus, we can conclude that a decrease in diameter leads to energetic instability in MgH_2 and magnesium nanowires; however, MgH_2 nanowires are more strongly destabilized than magnesium nanowires, which result in the thermodynamic destabilization of MgH_2 nanowires as their diameter decreases. Accordingly, the nanowire structured Mg can be considered as a promising hydrogen storage material due to its thermodynamic destabilization.

4.2.3 Nanofilms. Compared with other methods, 2D thin film fabrication provides a promising approach to achieve accurate control of the nanostructure, composition, and interfacial properties of hydrogen storage materials by accurately tailoring on the nanoscale. Consequently, thin films have been extensively applied in Mg-based hydrogen storage materials. 2D nanostructured Mg films were synthesized through different techniques such as electron beam evaporation, direct current (DC) and radio frequency (RF) magnetron sputtering deposition, and plasma sputter and pulsed laser deposition. Jain et al. summarized the advantages of pure Mg films and Mg multilayered films. Thin films offer an alternative approach for producing nano-structured materials with better control over morphology, stoichiometry and contamination.[23] Herein, we further review the role of nanofilms on the thermodynamic destabilization of MgH_2 with more new evidence.

Thermodynamic destabilization of MgH_2 via mechanical methods was first reported by Fujii.[61] As shown in Fig. 16(a), the contraction of PdH_x layers to Pd upon heating induced a large compressive stress in the lattice of MgH_2. The intrinsic stress is well correlated to grain size, where an increase in grain size accommodates a reduction in stress. In the Pd/Mg/Pd layered films fabricated by sputtering, the Mg layer was composed of fine columnar structures along the c-axis with a diameter in the
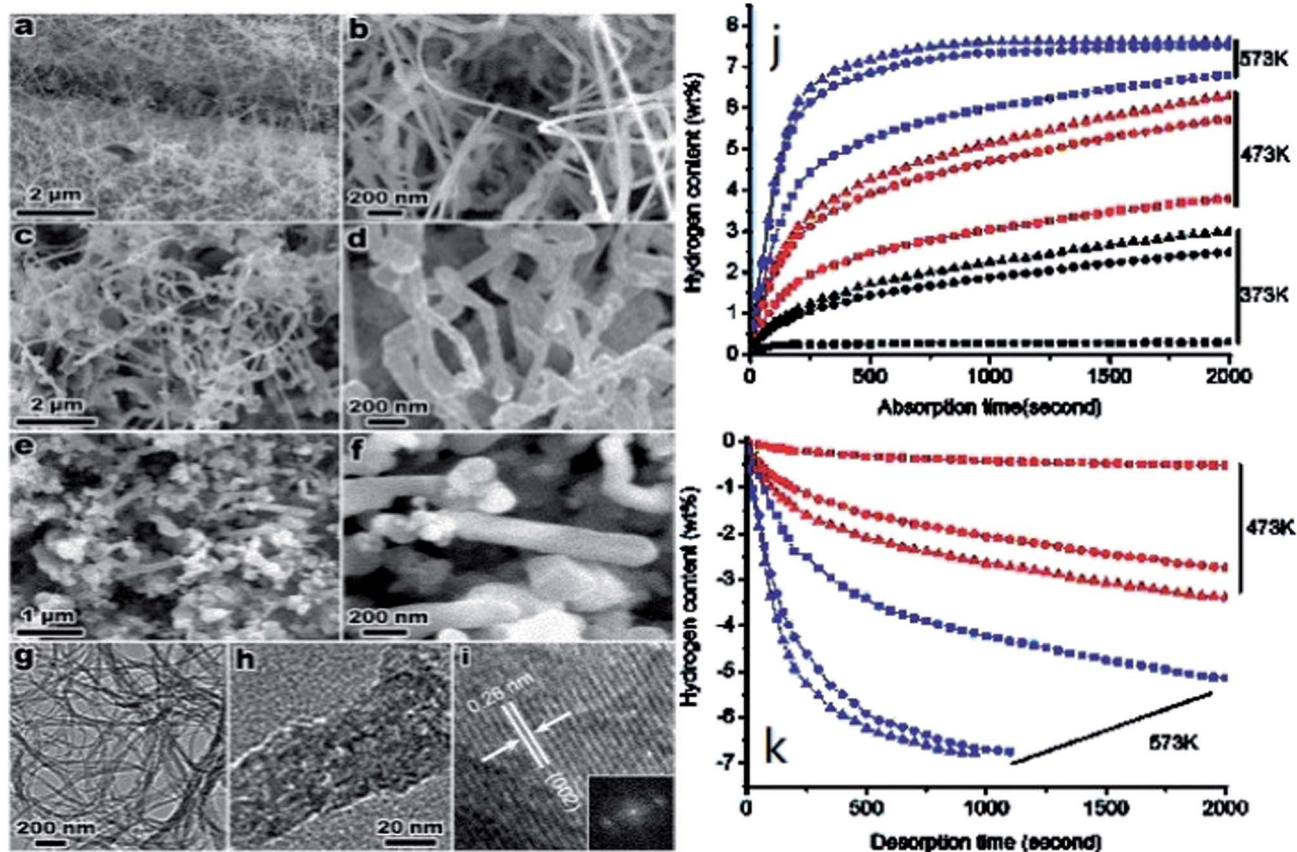
Fig. 14 Scanning electron microscopy (SEM) images of the Mg nanowires: (a and b) 30–50 nm, (c and d) 80–100 nm, and (e and f) 150–170 nm. TEM (g and h), and HRTEM (i) images of (a and b) with the corresponding fast Fourier transform (FFT) pattern (inset). Hydrogen absorption (j) and desorption (k) of the Mg nanowires (sample 1, triangles; sample 2, circles; and sample 3, squares) at different temperatures.[59]
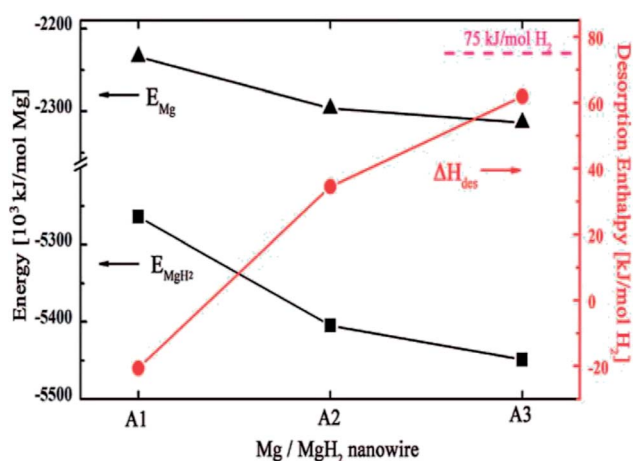

Fig. 15 Desorption enthalpy for MgH_2 nanowires (red line) and the size effect of the calculated energies for magnesium (triangle) and MgH_2 (tetragon) nanowires.[60]

range of 10–30 nm (Fig. 16(b)). This produced a large thermodynamic shift in the stability of MgH_2 and reduced its sorption temperature to just above room temperature (measured in vacuum), which can be attributed to the cooperative

phenomenon due to the elastic interaction between the nanostructured Mg and Pd layers.[62]

Subsequently, the hydrogen storage characteristics of multi-layer Mg nanofilms have been investigated intensively. MmM_5/Mg multi-layer thin films were deposited on a (0 0 1) Si substrate by direct current magnetron sputtering with a dual-target, and an advanced study proved that the apparent absorption of hydrogen in the Mg layer occurs at temperatures higher than 473 K and that the hydrogen absorbed can be fully released at 523 K.[63] Nanostructured Mg thin films grow in the shape of closely-stacked columns extending throughout the film thickness, while containing polycrystalline grains and grain boundary defects, which is responsible for the significant reduction in sorption temperature from 670 to 475 K by capping the Mg films with a thin Pd layer.[64] Other studies proved that thermodynamic properties and cycle stability of Mg–Al–Ti thin films or Mg–Cr–V films are significantly improved compared with pure MgH_2.[65,66]

Baldi *et al.*[67] revealed that the absorption plateau pressure can be altered when very thin layers of Mg are capped with a miscible element (Fig. 17). They assumed that the origins of this effect is due to 'elastic constraints', in accord with Fujii *et al.*, meaning that the volume change in MgH_2 is effectively restricted due to the small layer of alloying at the interface. The fundamental reasoning for this effect is the repulsive attraction
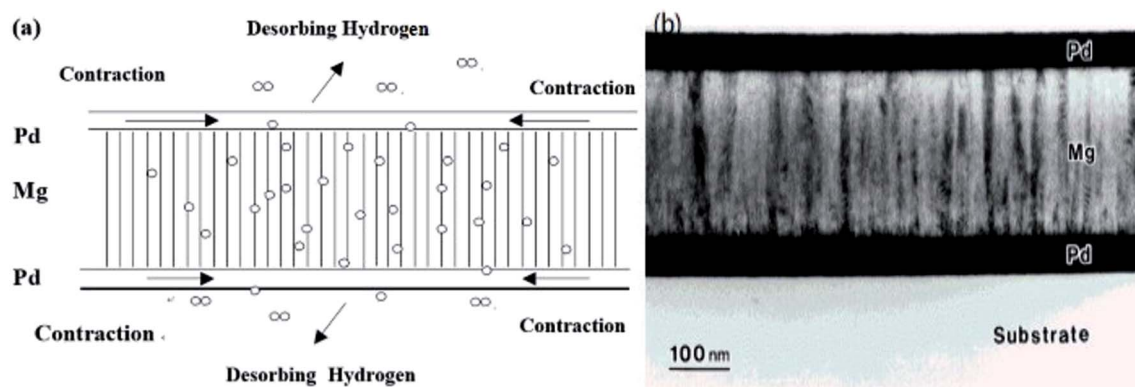
Fig. 16 Schematic representation of the co-operative phenomenon (a) and TEM micrographs of the cross-section of Pd (50 nm)/Mg (200 nm)/Pd (50 nm) films before hydrogenation (b).[61,62]
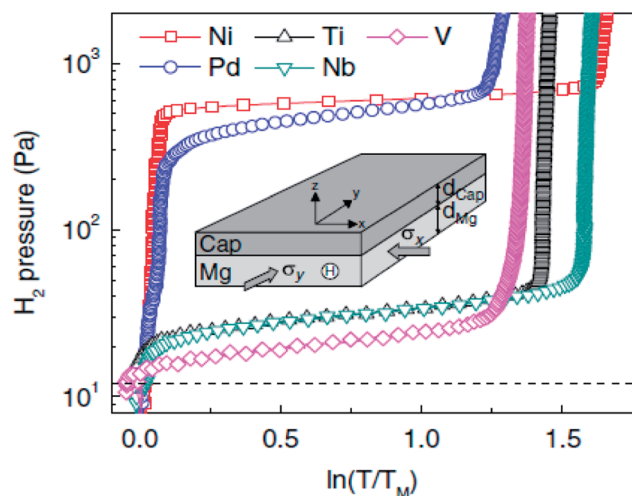

Fig. 17 Effect of cap layer: PTI measured at 333 K for Ti(10 nm)Mg(20 nm)X(10 nm)Pd(10 nm) samples deposited on glass with X = Ni, Pd, Ti, Nb, and V.[67]

between the H–H atoms within metals when volume expansion is restricted. Chung et al.[68] argued that the observed destabilization has a chemical origin, whereby the interfacial mixing of the Mg/Pd regions requires additional energy for the formation of MgH_2, which is exacerbated within thinner layers. In addition, Mooij et al. revealed that at very small thicknesses, the interface energies from adjacent layers become more important by synthesizing a wedge shaped Mg film with a thickness varying between 1–10 nm.[69] Hughes et al.[70] provided new insight into the destabilization mechanism by investigating the influence and comparative differences of Ti- and Y-based multilayers. It was remarkable that the Ti multilayers showed some destabilization with thinner layers down to 10 nm, which is proposed to be due to interfacial energy contributions. In comparison, Mg/Y-based multilayers can provide a new route towards MgH_2 destabilization due to the accommodation of lattice mismatch between the strained FCC Y/Mg interfaces.

4.2.4 Nanoconfinement. Nanoconfinement is an efficient route to hinder the particle growth and agglomeration of hydride particles within the supporting material and significantly improve the cycling property affected by the direct synthesis of nanostructured hydrides. A high-surface-area, nano-porous support for the active phase can facilitate the preparation of small particles and stabilize the particle size during heat treatments or cycling. In general, for hydrogen storage materials, the specific requirements for the matrix include light-weight, high loading of the active materials, not reactive towards the active materials, low-cost and abundant, such as carbon-based materials, organic polymers and ordered mesoporous oxides.

Recently, magnesium nanoparticles confined in carbon aerogels (CA) have attracted much attention.[71–73] Liu et al.[72] reported magnesium nanoparticles confined in carbon aerogels through the hydrogenation of infiltrated dibutyl-magnesium followed by hydrogen desorption at 623 K, which has a size in the range of 5.0 to 20.0 nm. The hydrogenation and dehydrogenation enthalpies of the confined Mg were determined to be 65.1 ± 1.56 kJ $(mol^{-1}\ H_2)$ and 68.8 ± 1.03 kJ $(mol^{-1}\ H_2)$, respectively. Jia et al.[74] prepared the MgH_2@CMK-3 nanoconfinement system and experimentally realized low temperature hydrogen release starting from 323 K. Comparing the calculated reaction energy (E_r) of clusters of pure MgH_2 and MgH_2/C (Fig. 18), they concluded that the interfacial effect can effectively improve the low-temperature release properties of MgH_2 clusters, even if the cluster is not ultra-small (Fig. 18c). Consequently, they proposed a new mechanism for destabilizing Mg–H bonding via the combination of the size effect and MgH_2–carbon scaffold interfacial bonding, which is more superior than nanoparticles or 2D films.

Modifying the surface of NPs with a gas-selective outer layer of polymer or elemental metal has been well demonstrated to be a feasible route to obtain superior gas-selective permeability and structural stability. Jeon et al.[75] reported the synthesis of an air-stable composite material consisting of metallic Mg nanocrystals (NCs) in a gas-barrier polymer matrix, which enabled them to absorb and release hydrogen without oxidation
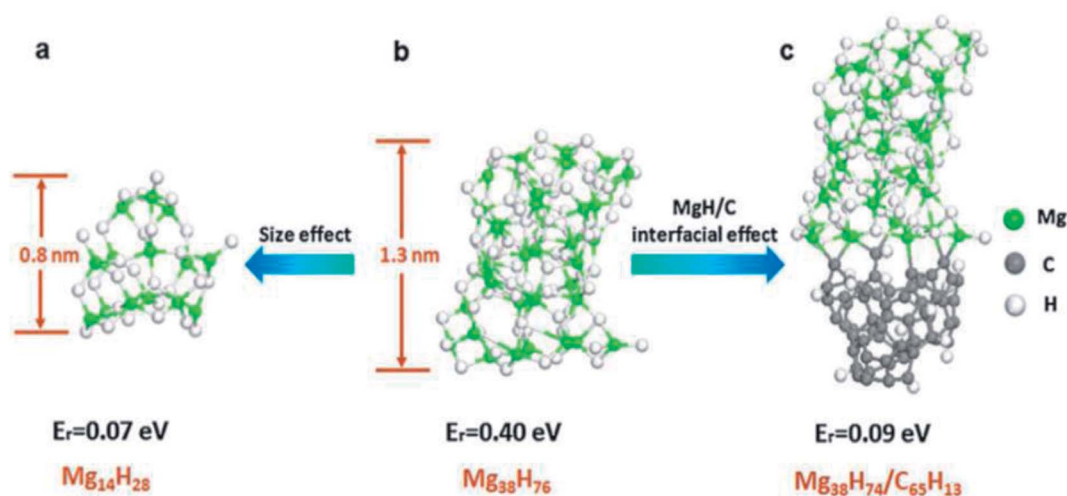
Fig. 18 Reaction energy (E_r) for hydrogen release from clusters of pure MgH_2 and MgH_2/C. (a) $Mg_{14}H_{28}$ cluster, (b) $Mg_{38}H_{76}$ cluster, and (c) $Mg_{38}H_{74}$ adsorbed on a cluster of amorphous carbon.[74]

(Fig. 19(a)). The average Mg NCs diameter was 4.9–2.1 nm (Fig. 19(b)) and the composite material enabled both the storage of a high density of hydrogen (up to 6 wt% of Mg and 4 wt% for the composite) and rapid kinetics (loading in <30 min at 473 K) (Fig. 19(c)). Moreover, nanostructuring of Mg results in rapid storage kinetics without using expensive heavy metal catalysts. Besides, graphene nanosheets and gas-selective reduced graphene oxide (rGO) have received much attention due to their high hydrogen selectivity.[76,77] Cho et al.[78] reported the development of similar materials, which were comprised of nickel-doped Mg nanocrystals encapsulated by molecular-sieving reduced graphene oxide (rGO) layers, with simultaneously high hydrogen storage capacity (6.5 wt% for the total composite) and excellent kinetics, while maintaining robustness. Overall, this approach of synthesizing nanosized air-sensitive metal nanocrystals protected in a gas-selective polymer provides new opportunities for low-cost high-capacity hydrogen storage media, batteries and fuel cells.

Remarkably, Cui et al.[79] provided another way to successfully load Mg into the nano-sized pores of an anodic aluminum oxide (AAO) template for realizing the nano-confinement of Mg via

vapor transport deposition with a slight reduction in the hydrogen desorption enthalpy of MgH_2 from (74.42 ± 0.12) to (73.21 ± 0.04) kJ (mol^{-1} H_2). There was more evidence for the reduction in desorption temperature when MgH_2 was embedded within an LiCl salt matrix.[80] The particle size of 7 nm showed a reduction in desorption temperature of 6 K. Although this is smaller than expected, it shows the possibility of destabilization.

Over the past few decades, the thermodynamic destabilization mechanisms of nanostructured materials for hydrogen storage applications have been well demonstrated, including size effects, lattice strain, interface energies, elastic constraints, and combination of the size effect and interface energies. Remarkable advances have been achieved in destabilizing thermodynamics by taking advantage of the above mechanisms. However, there is an urgent need to address the agglomeration of particles in support-free nano-scaled hydrides or nanowires since it results in collapse of the nanostructure after repeated hydrogen uptake and release cycles, which is still a significant challenge. It is generally accepted that nano-confinement leads to an obvious loss in the gravimetric
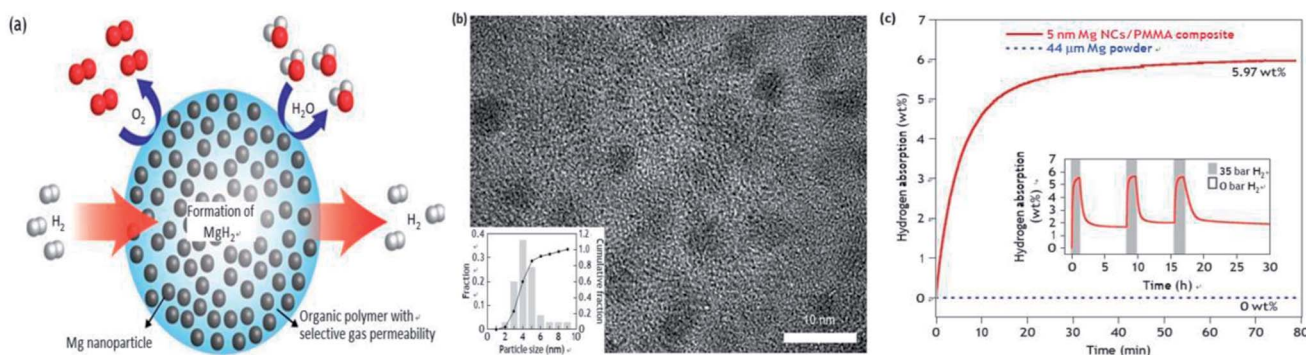

Fig. 19 (a) Schematic of hydrogen storage composite material: high-capacity Mg NCs are encapsulated by a selectively gas-permeable polymer, (b) HRTEM of the nanocomposite and particle size distribution of Mg in the polymer matrix, and (c) hydrogen absorption kinetic analyses of bulk Mg and Mg/PMMA composites at 473 K and 35 bar hydrogen.[75]

hydrogen storage capacity compared with that of MgH_2 and the low loading of Mg NPs is still a big problem. Besides, the synthesis of nanostructured materials is another challenge for practical applications.

4.3 Metastable phases

Many groups have reported the preparation methods, crystal structures, thermodynamic properties and hydrogen desorption paths of γ-MgH_2. Generally, high-pressure phase γ-MgH_2 can be obtained by heating α-MgH_2 (ref. 81) or BM α-MgH_2.[82] The deuterium atoms surround magnesium in a distorted octahedral configuration with bond distances of Mg-D = 1.915(3), 1.943(3) and 2.004(3) Å.[82] The thermodynamic properties of γ- and β-MgH_2 have also been determined by the first-principle calculations, where the supercell based on the γ-MgH_2 (1 1 0) plane is the most unstable with a surface energy of 1.23 J m^{-2} and dehydriding enthalpy change of 44.66 kJ mol^{-1}, while that of the β-MgH_2 (1 1 0) plane has a surface energy of 0.19 J m^{-2} and enthalpy change of 78.16 kJ mol^{-1}. This is because in γ-MgH_2, the H octahedrons surrounding the Mg atoms are deformed and the octahedron chain takes a zigzag form instead of the straight chain in the β phase.[12] Thus, we can conclude that conversion to the metastable γ-MgH_2 phase should lead to improved hydrogen sorption properties and provide another approach to modify the thermodynamics of Mg-based materials. However, irreversible reconversion of the γ-phase into the β-phase[83] or Mg[84] occurs during heat treatment at 583 K in 1 bar hydrogen atmosphere.

Numerous researchers have shown that ball milling is an efficient way to obtain a high proportion of γ-MgH_2. Zhou *et al.*[12] prepared magnesium hydride *via* reactive milling under a hydrogen atmosphere using carbon as a milling aid. The enthalpy change determined by experimental isotherms gradually decreased with more γ-MgH_2 from a longer milling time. They also found that the unstable γ-MgH_2 in the as-milled material disappeared during desorption/absorption cycle. Xiao *et al.*[83] made use of a simple wet chemical route by ball milling MgH_2 with LiCl as a PCA at room temperature followed by tetrahydrofuran (THF) treatment under an Ar atmosphere to obtain a magnesium hydride composite (MgH_2-E), which was composed of 18 wt% orthorhombic γ-MgH_2 with particle lengths/widths ranging from 50–400 nm. The β-/γ-MgH_2 nanocomposite exhibited a dehydrogenation capacity of 6.6 wt% and started to release hydrogen at 533 K (Fig. 20), which can be attributed to both the existence of the MgH_2 nanostructure and the presence of γ-MgH_2. However, they failed to determine the hydrogen desorption path of γ-MgH_2 due to the limited available data and experimental methods.

Shen *et al.*[85] reported the electrochemical synthesis of nanosized Mg, leading to the formation of a mixed γ/β hydride phase upon hydrogen absorption with a high γ-MgH_2 content (29.6%) with a crystallite size of 10.9 ± 0.7 nm. High-resolution transmission electron microscopy (HRTEM) also locally confirmed the formation of γ- and β-MgH_2 (Fig. 21(b)), and this indicated that individual magnesium particles may contain both phases. As shown in Fig. 21(a), the decomposition of γ-
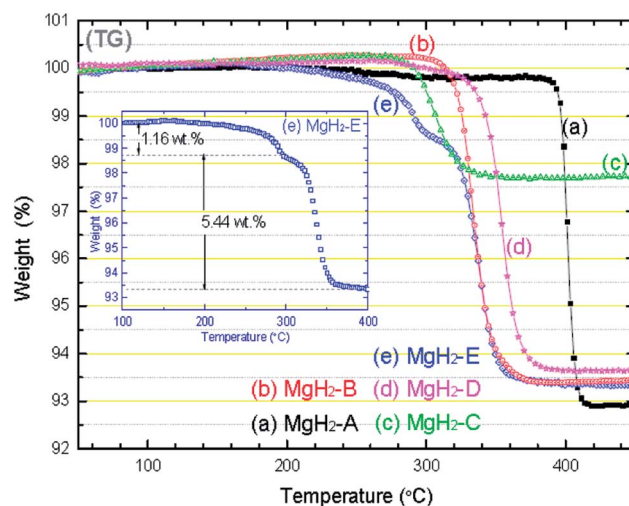

Fig. 20 TG-DTA curves of (a) MgH2-A, (b) MgH2-B, (c) MgH2-C, (d) MgH2-D, and (e) MgH2-E samples. The heating rate was 2 °C min^{-1} from room temperature to 450 °C in each case. The inset shows the detail of the mass loss profile for MgH2-E.[83]

MgH_2 starts the same time as that of β-MgH_2 with the simultaneous generation of hexagonal Mg. Thus, it is evident that both phases are intrinsically linked and γ-MgH_2 may trigger the decomposition of β-MgH_2. The presence of γ-MgH_2 was found to cause a significant reduction in the apparent activation energy from 106.2 ± 4.0 to 69.1 ± 2.9 kJ mol^{-1} and a reduction in the reaction enthalpy from 74.8 ± 1.0 to 57.7 ± 5.3 kJ (mol^{-1} H_2). It is notable that metastable γ-MgH_2 has potential to lead to better kinetics and thermodynamic properties for the Mg/MgH_2 system. This is consistent with the study conducted by Ponthieu,[86] in which for Ti-containing nanocomposites, both γ- and β-MgD_2 desorbed simultaneously above 475 K together with a concomitant increase in the Mg phase according to the reaction (7):

$$x(\gamma\text{-}MgH_2) + (1 - x)(\beta\text{-}MgH_2) \rightarrow Mg + H_2 \qquad (7)$$

The results show that the presence of γ-MgH_2 destabilizes the β-MgH_2 phase and shows a synergetic effect during hydrogen desorption, reducing the β-MgH_2 desorption temperature.[87]

Considering the achieved progress, although γ-MgH_2 can be synthesized by heating the low-pressure phase, ball milling or hydrogenation of nanosized Mg and alter the thermodynamic properties of Mg/MgH_2 without loss in its hydrogen storage capacity, the problems of bad cycle performance under high temperature and low proportion of γ-MgH_2 still need to be addressed in further studies. However, it is promising that γ-MgH_2 can exist stably with a decrease in desorption temperature and increase of proportion of γ-MgH_2. Besides, Song *et al.*[88] predicted a metastable phase of MgH_2 by first principle calculations, where the metastable phase has a tetragonal symmetry ($I4_1/amd$, group 141) and meets all the mechanical stability criteria, and its formation enthalpy is −58.03 kJ mol^{-1} H_2.
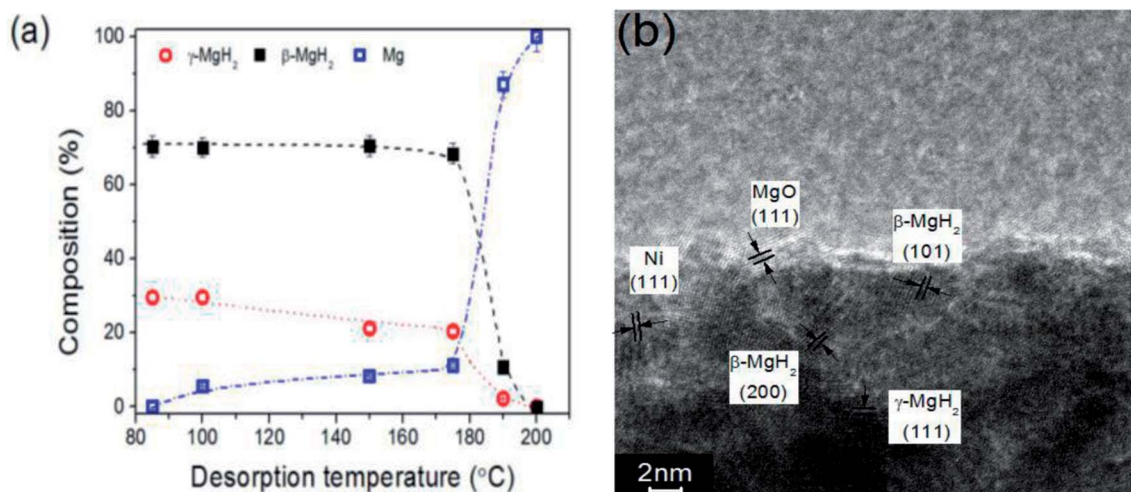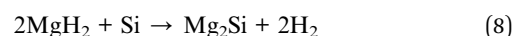
Fig. 21 Thermal stability of γ-MgH$_2$ during hydrogen desorption as function of desorption temperature (a) and HRTEM images of electro-synthesized Mg after hydrogen absorption at 100 °C (b).[85]

Hence, the tetragonal structure is more desirable than α-MgH$_2$ for practical hydrogen storage applications. However, this needs to be further confirmed by experimental data.

4.4 Changing reaction pathway

Fig. 22 shows a general enthalpy diagram illustrating the destabilization of a strongly bound hydride through the addition of a reactive additive.[89] The alloying additive, B, reduces the dehydrogenation enthalpy through the formation of AB$_x$ and effectively destabilizes the hydride, AH$_2$. This reaction occurs with a reduced enthalpy and therefore, increases the equilibrium pressure and decreases the dehydrogenation temperature.

An intensively system investigated is the MgH$_2$–Si system, in which, Mg$_2$Si forms upon dehydrogenation according to reaction (8):

Fig. 22 Generalized enthalpy diagram illustrating destabilization through alloy formation upon dehydrogenation.[89]

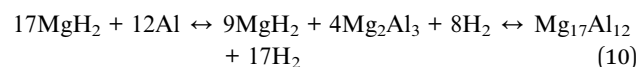$$2MgH_2 + Si \rightarrow Mg_2Si + 2H_2 \qquad (8)$$

Thermodynamic calculations indicate the 1 bar equilibrium pressure is at approximately 293 K and 100 bars at approximately 423 K. Thus, it is concluded that the MgH$_2$/Si system, with a hydrogen capacity of 5.0 wt%, is practical for hydrogen storage at reduced temperatures. Hence, alloying Si with MgH$_2$ is supposed to significantly destabilize the Mg–H bond with the enthalpy reduced to 41 kJ (mol^{-1} H$_2$) due to the formation of Mg$_2$Si in eqn (8).[90] However, the re-hydrogenation of Mg$_2$Si was found to be severely limited by the reaction kinetics and the mass transport of Mg and Si into separate phases.[91,92] Gennari et al.[93] found that the presence of Ge decreases the hydride decomposition temperature in the range of 323 to 423 K, which was prepared by mechanical milling. Meanwhile, Walker et al.[94] started with MgH$_2$ and milled it with Ge under an Ar atmosphere to prepare Mg$_2$Ge (eqn (9)).

$$2MgH_2 + Ge \rightarrow Mg_2Ge + 2H_2 \qquad (9)$$
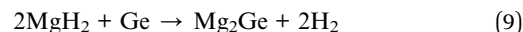
Their results showed that Ge acts as a thermodynamic destabilization agent for MgH$_2$, resulting in a dramatic decrease in the ΔH of dehydrogenation to 14 kJ (mol^{-1} H$_2$). This dramatically reduced the temperature of dehydrogenation to 403 K, but unfortunately, the desorption product Mg$_2$Ge could not absorb hydrogen to form MgH$_2$ and Ge. In addition, the additives Si and Ge cannot form hydrides; thus, the hydrogen capacity was partially lost.

Aluminum also forms stable compounds or alloys with Mg, such as Mg$_{17}$Al$_{12}$ (γ phase) and Mg$_2$Al$_3$ (eqn (10)).

$$17MgH_2 + 12Al \leftrightarrow 9MgH_2 + 4Mg_2Al_3 + 8H_2 \leftrightarrow Mg_{17}Al_{12} + 17H_2 \qquad (10)$$

However, the destabilization effect of this systems is rather small (only about 50 K decrease in decomposition start temperature), and the theoretical hydrogen content of MgH$_2$–Al
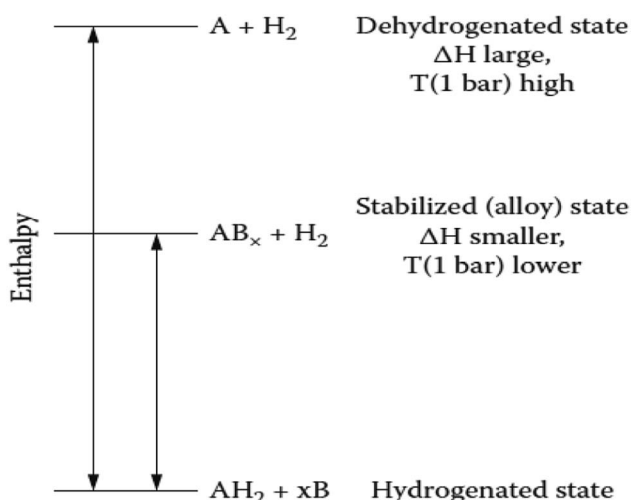
can reach 4.4 wt% with a small decrease in the desorption enthalpy ΔH of 6 kJ (mol^{-1} H$_2$).[95] The reversible hydrogenation was accomplished in three transformation steps (Fig. 23), where initially, only Mg reacts and forms MgH$_2$, then the γ-Mg$_{17}$Al$_{12}$ phase is decomposed into the Mg-poor β-Mg$_2$Al$_3$ phase. Finally, the Mg-hydride phase is fully formed from the resulting Mg$_2$Al$_3$.[96]

Significant progress has been achieved to alter the hydrogen storage properties of Mg-based materials, where their ΔH undergoes a great decrease through alloying, nanostructuring, forming metastable phases and changing the reaction path, as shown in Table 4. However, none of these strategies totally satisfy the requirements of practical applications; thus, so further studies on the thermodynamic properties of Mg/MgH$_2$ need to be performed to realize the practical application goals by DOE (Table 1). The future looks bright for the combination of alloying, nanostructuring, and metastable phase.

5. Novel Mg-based composite materials

Altering the thermodynamic properties of Mg/MgH$_2$ *via* a single measure cannot satisfy the requirements for its practical application. Therefore, the introduction of appropriate metal hydrides/dopants was proposed to further modify its thermodynamic properties. The widely studied Mg-based composites include Mg–Ni–RE,[97–99] Mg–Ni–Ti,[100] MgH$_2$–LiBH$_4$,[101] LiNH$_2$–MgH$_2$,[102] LiBH$_4$–Mg$_2$NiH$_4$,[103] and MgH$_2$–NaAlH$_4$.[104]

5.1 Amorphization

Amorphization as a novel method can alter the hydrogen storage properties of Mg-based materials with more specific octahedral and/or tetrahedral sites for hydrogen occupation and extra potential vacancies for hydrogenation. Mg–RE–Ni

amorphous alloys prepared by melt-spinning are typical examples with a hydrogen density as high as 5.5 wt% at 573 K, and the microstructure of the as-spun alloys consist of an amorphous matrix containing MgH$_2$, Mg$_2$NiH$_4$ and REH$_x$.[97] Lin *et al.*[98] found that the Mg–Ce–Ni metallic glasses (MGs) can reversibly absorb and desorb about 0.2–0.4 wt% H at room temperature without activation, and the hydrogenation capacity of the glassy Mg-based alloy is twice that of the corresponding crystalline alloy due to its free volume and disordered atomic structure.

Recent studies showed that desirable properties can realized by combining crystalline and amorphous materials, which are better than that of the amorphous counterpart. Due to the combination of nanocrystalline magnesium matrix and the amorphous nickel inter-grain region, Mg–Ni nano/amorphous composite materials are superior over their amorphous counterpart in hydrogen storage capacity and kinetics.[99] Besides, it was also found that Mg–Ni–La nano/amorphous composite materials with the starting temperature of hydrogen desorption from 473 K to 298 K have better properties than their Mg 50%–Ni 50% composite material. This indicates that the thermodynamic stability of Mg–Ni nano/amorphous composite materials can be reduced by additives such as La.[99] Another research reported that the nanostructured 50% Mg$_{1.5}$Mn$_{0.5}$Ni/50% LaNi$_{3.75}$Mn$_{0.75}$Al$_{0.25}$Co$_{0.25}$ composite material can release H$_2$ at room temperature as a result of the combined engineering of many factors, including alloying, surface properties, microstructure, grain size and others.[105]

5.2 Novel reactant mixtures

The U.S. Department of Energy Metal Hydride Center of Excellence (MHCoE) conducted substantial research into new reversible hydrogen storage materials for light-duty vehicles, which is composed of three main fields: mechanisms and modeling, materials development, and system design and materials engineering.[106] Alapati *et al.*[102] theoretically predicted the LiNH$_2$ + MgH$_2$ (1 : 1) system due to its very attractive theoretical desorption enthalpy of ΔH = 32 kJ (mol^{-1} H$_2$), with a hydrogen capacity of 8.2 wt% by the following reaction:

$$MgH_2 + LiNH_2 \rightarrow LiMgN + 2H_2 \qquad (11)$$
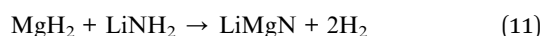
The high predicted weight percentage of hydrogen is due to its full dehydrogenation to LiMgN, bypassing the undesirable imide intermediate, as shown in Fig. 24. Based on this, substantial work has been done to demonstrate the feasibility of reaction (11) experimentally.[107–109] The total weight loss was 8.1 wt% of the initial weight after the sample was held at 493 K for 20 min, with a ΔH of 33.5 kJ mol^{-1} H$_2$, which is very close to the theoretically predicted reaction enthalpy.[110] However, its application has been greatly hindered by its rather high activation energy barriers.

Based on these results, Dolotko *et al.*[111] demonstrated thermochemical transformations in 2MNH$_2$–3MgH$_2$ systems (M = Li or Na). A total of 6.45 wt% of hydrogen was released by the 2LiNH$_2$–3MgH$_2$ system beginning at 459 K, and a total of
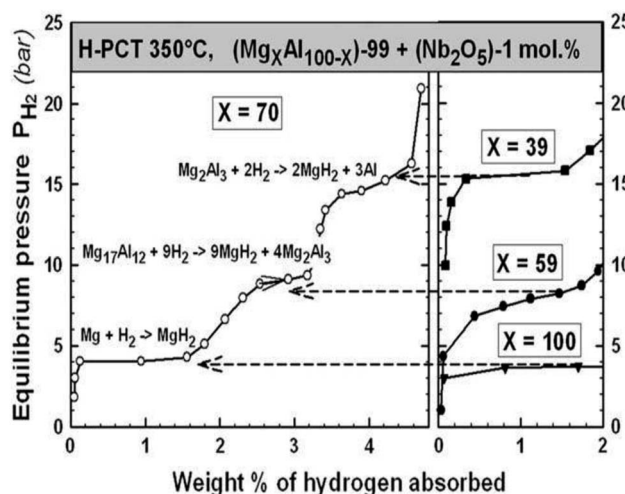

Fig. 23 Summary of the PCT absorption curves of the (Mg$_X$Al$_{100-X}$) − 99 + (Nb$_2$O$_5$) − 1 mol% samples. The 3 steps of transformation from the X = 70 samples are compared to the absorption curves of the X = 100 (Mg), X = 59 (Mg$_{17}$Al$_{12}$) and X = 39 (Mg$_2$Al$_3$) compounds.[96]

Table 4 ΔH and hydrogen storage capacity of Mg-based hydrogen materials

Strategy	Material	Synthetic method	$|\Delta H|$ (kJ (mol^{-1} H$_2$))	H$_2$ capacity (wt%)	Ref.
Alloying	Mg$_2$NiH$_4$	Mechanical alloying	64	3.6	29
	Mg–Cu–H	Hydrogen-plasma-metal reaction	67.5	2.6	34
	(Mg$_{0.68}$Ca$_{0.32}$)Ni$_2$	Induce furnace melting	37	1.4	32
	Mg$_{0.9}$In$_{0.1}$	Ball milling	65	4.2	44
Nanostructuring	MgLi$_{4.6}$Napth$_{0.5}$	Electrochemical reduction	63.5	3.4	51
	MgH$_2$–0.1TiH$_2$	Ball milling	68	6	52
	MgH$_2$–C	Ball milling	44.5	5.2	55
	La$_2$Mg$_{17}$–LaNi$_5$	Mechanical milling	53.23	4.9	58
	Mg nanowires	Vapor-transport approach	65.3	7.6	59
	Mg–carbon aerogels	Solution impregnation	65.1	2.35	72
	MgH$_2$@CMK-3	Solution impregnation	55.4	6	74
Metastable phase	γ-MgH$_2$ (1.99 wt%)	Ball milling	45.03	5	12
	γ-MgH$_2$ (29.6 wt%)	Electrochemical synthesis	57.7	3.5	85
	T-MgH$_2$	First principles calculations	58.04	—	88
Changing reaction pathway	MgH$_2$–Si	Ball milling	41	5	90
	MgH$_2$–Ge	Ball milling	14	3	94
	MgH$_2$–Al	Mechanical alloying	68	4.4	95
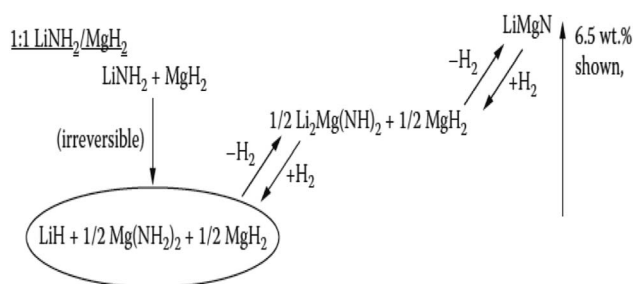
Fig. 24 Mechanism for hydrogen absorption/desorption of 1 : 1 LiNH$_2$/MgH$_2$.[102]

5.1 wt% H$_2$ was released by the 2NaNH$_2$–3MgH$_2$ system starting at 403 K according to the following solid state transformation:

$$2MNH_2 + 3MgH_2 \rightarrow Mg_3N_2 + 2MH + 4H_2\uparrow \quad (12)$$
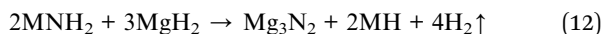
Other groups further studied LiNH$_2$–nMgH$_2$ (n = 0.5, 0.7, 0.9, 1.0, 1.5 and 2.0) nanocomposites to shed light on the combined effects of molar ratio and ball milling energy on the phase transformations and mechanical dehydrogenation.[112,113] For all molar ratios, n, the hydride nanocomposites are fully reversible at 448 K under a relatively mild pressure of 50 bar H$_2$. To further decrease the de-/re-hydrogenation temperature of the Li–Mg–N–H system, Xia et al.[114] reported a novel multi-reaction methodology for the synthesis of nanosized Li$_2$Mg (NH)$_2$ space confined in thin-film hollow carbon spheres (THCSs) with a uniform dispersion, resulting in a stable cycling capacity and reversible hydrogen sorption at a temperature of 378 K. Besides, Zhang et al.[115] reported a brief review of the state-of-the art advances in improving the performances of the lightweight complex hydride Li–Mg–N–H system. Due to nano effects, the space-confinement and nanoconfinement seem to be more effective for improving the hydrogen storage performance, and it is significant to develop hydrogen storage materials by studying the nano-confined effects on the Li–Mg–N–H systems.

Besides the Li–Mg–N–H system, Vajo et al.[103] studied the LiBH$_4$/Mg$_2$NiH$_4$ system due to its unique features, including full reversibility, reaction through a direct low temperature kinetic pathway, formation of a unique ternary boride phase (MgNi$_{2.5}$B$_2$), and low reaction enthalpy coupled with low entropy. The reaction begins at temperatures as low as 523 K, which is possibly due to the catalytic nature of Ni in the NiH$_4{}^{2-}$ anion and is superior than MgH$_2$–LiBH$_4$.[101] Thus far, this system appears to be the only reversible destabilized system that reacts through a direct reaction pathway. However, its capacity (2.6 wt%) for the direct low temperature step shown above is too low for practical use.

5.3 Synergistic effect

Recent research has shown that the synergistic effect, which exists in the γ/β hydride phase or multi-layer Mg nanofilms induced by elastic constraints or interface energies, can effectively alter the desorption temperature of Mg/MgH$_2$, but this effect has not been observed directly in powders because the metal lattice is often free to expand. However, nano Mg-based composite materials prepared by ball milling have proven that the synergistic effect produced by the high density interface between different phases can further enhance the adsorption/dehydrogenation process, as shown in Fig. 25. The desorbing phase may be surrounded by an alternative phase and the tensile/compressive stress placed on the adjacent phase then acts as a driving force for destabilization. Significant investigations have been undertaken to improve the hydrogen storage properties of Mg toward the requirements of practical applications, including Mg–Mg$_2$Ni,[116] Mg–Ni–RE,[117] Mg–TiCrV,[118–120] Mg–LaNi$_x$,[121,122] and Mg–TiB$_2$/graphene nanosheets (GNSs).[123]

Zaluska et al.[116] reported the synergistic effects of desorption for mixtures of Mg$_2$NiH$_4$/MgH$_2$ phases prepared by ball-milling. The DSC results of the mixtures showed that they could operate
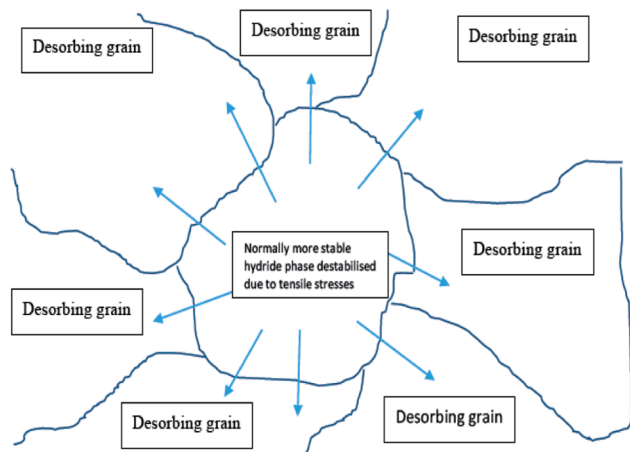
Fig. 25 Schematic representation of the potential synergistic effects observed in multiphase powders.[70]

at temperatures of 493–513 K. Li et al.[117] prepared an Mg-20 wt% Ni–Y composite by reactive mechanical alloying (RMA), and the MgH_2 and Mg_2NiH_4 phases co-existed in the milled composite. They found that the dehydrogenation temperature of the Mg-20 wt% Ni–Y composite was depressed by about 100 K compared to that of the milled pure MgH_2 due to the co-contribution of the synergetic effect of hydrogen sorption of

MgH_2 and Mg_2NiH_4 and many crystal defects created by the RMA. This proves that mechanically-treated hydrides offer a new opportunity for Mg-based materials, exploiting the high capacity of magnesium hydride while operating at a much lower temperature than conventional MgH_2.

Different from the synergistic effect resulting from elastic instability, Lim et al.,[124] for the first time, prepared Mg nanocrystals embedded in a metal–organic framework (MOF). The Mg@SNU-9′b sample was loaded with 6.52 wt% Mg NPs with a diagonal hexagon length ranging from 44–88 nm (Fig. 26(b)). They demonstrated that Mg–NCs@MOF is a hybrid-hydrogen-storage material that has both physical adsorption and chemisorption properties, and exhibits synergistic effects to increase the isosteric heat of H_2 physisorption and to decrease the temperatures for the chemisorption/desorption of H_2. Although the hydrogen storage capacities of Mg NCs@MOF were rather low at high temperature (0.2 wt% and 0.24 wt% at 325 K and 415 K, respectively) as shown in Fig. 26(d and e), the study of hybrid-hydrogen-storage material provides another new strategy for H_2 storage and transport for the future.

Substantial Mg-based composite materials have been found by combining theoretical predictions and experimental approaches. Furthermore, the mechanism of altering the hydrogen storage properties of Mg/MgH_2 can be attributed to the advantages of combining many strategies including
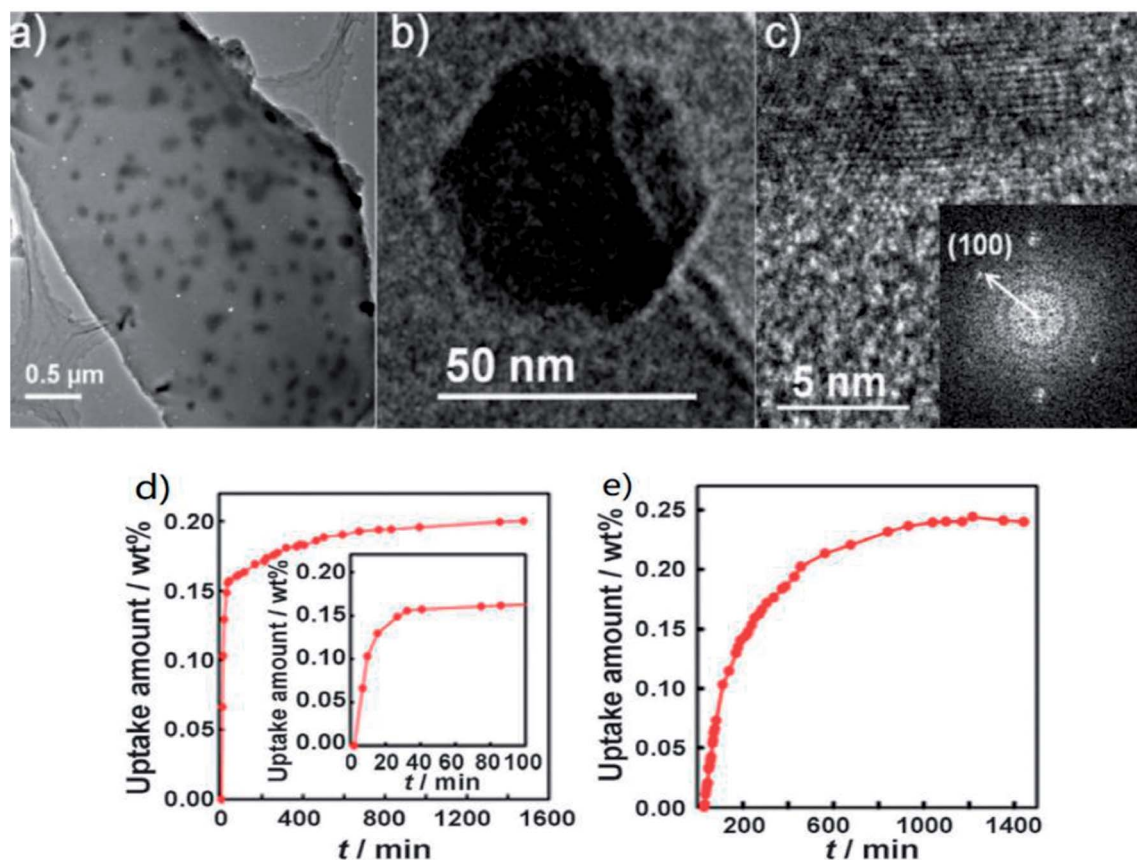

Fig. 26 High-resolution transmission electron microscopy (HRTEM) images of (a) Mg@SNU-9′b, (b) hexagonal-shaped Mg nanocrystal and (c) its edge image showing the lattice fringe (100) d-spacing of Mg^0 (2.7782 Å, JCPDS 04-0770). Inset: selected-area electron diffraction (SAED) pattern. H_2 absorption kinetics of Mg@SNU-9′c at (d) 325 K and 80 bar and (e) 415 K and 40 bar.[124]

alloying, surface properties, nanostructuring, synergistic effect and others, which holds potential as an on-board storage material for light-duty vehicles with a high hydrogen capacity and low desorption temperature.

6. Conclusion and outlook

Hydrogen energy is the one ideal means of energy storage for transportation and conversion of energy, which holds the advantages of high gravimetric energy density and carbon-free energy carrier.[125] There is a generally accepted opinion that hydrogen storage materials and technologies are the key issues for the realization of a hydrogen energy economy. Among the hydrogen storage materials, magnesium-based alloys show great application prospect due to their high hydrogen storage capacity, low cost, high abundance and non-toxicity. However, they are severely limited by their high decomposition temperatures and/or poor reversibility due to unfavorable de-/hydriding thermodynamics and/or kinetics. Despite the significant progress achieved with respect to the kinetics of hydrogen absorption/desorption in magnesium, its stable thermodynamic property is still the main drawback, which hinders its practical applications.[126,127] In this review, we summarized the effective measures to alter the hydrogen storage properties of MgH_2, such as alloying, nanostructuring, metastable phase formation, changing reaction paths and synergistic effects. However, all of these strategies have limitations. Alloying and changing the reaction path are the traditional and effective ways to decrease the formation enthalpy; however, at the expense of hydrogen capacity and some reactions are irreversible. Nanostructuring is a good way to change the hydrogen storage properties, but the synthesis and poor stability of nanostructures remain challenging. γ-MgH_2 with a low formation enthalpy gradually disappears during the absorption/desorption cycle process. Considering the advantages and disadvantages of these strategies, consequently, a new strategy, nano Mg-based composite materials, was proposed, which combined the advantages of alloy engineering, nanostructuring, and synergistic effect created by the RMM, resulting in instability in the thermodynamic properties of Mg/MgH_2. However, there still a long way before the Mg/MgH_2 system meets the criteria stipulated by the DOE for light-duty vehicles.

Based on the substantial progress, further research on Mg-based material should focus on the following aspects:

(1) Novel preparation techniques require more attention. The synthetic approach is the first and most important step for the effective modification of the properties of Mg. Nowadays, mechanical milling, physical/chemical deposition, wet chemical routes, equal channel angular pressing and electrochemical approaches have been revisited for the synthesis of nanosized Mg. However, these approaches have failed in the advanced control over Mg atomic organization, crystalline-to-amorphous transitions, formation of metastable γ-MgH_2 phase and stabilization of specific nanostructures. Thus, new synthetic routes need to be developed to control the assembly of Mg atoms, content of different phases, and the location and level of doping of additives/catalysts.

(2) Finding a better way to stabilize nanostructuring. Promisingly, nanostructuring can effectively alleviate kinetic barriers and reduce thermodynamic stability. However, many challenges still exist in terms of serious aggregation and structure collapse during dehydriding/hydriding. The use of scaffolds hinders particle growth and agglomeration; however, it results in a significant capacity decrease. Therefore, new forms of stabilization should be explored to maximize the storage capacity, while providing effective stabilization for nanosized Mg without scaffolds, such as the introduction of modified graphene nanoribbons, introduction of a second phase, storing additional hydrogen and core–shell methods, should be pursued.

(3) Predicting novel Mg-based composite materials by combining theoretical methods and experimental approaches, which can efficiently combine the advantages of alloy engineering, nanostructuring, and synergistic effects. More attention should be paid to systematic theoretical research including crystallographic/structural quantities, enthalpy/entropy/surface energy, defect formation energies and computational spectroscopy, which can be used as guidelines for the preparation of new Mg-based hydrogen materials.

Ideal storage materials with low reaction temperatures, a reaction heat in the range of $|\Delta H| = 20$–30 kJ (mol^{-1} H$_2$) and an on-board reversible hydrogen storage density of more than 6 wt% H$_2$ have not been found. However, it is expected that significant breakthrough will realize the DOE's targets with more accurate fundamental guidance and more advanced technical approaches connecting targeted properties with material microstructures.

Conflicts of interest

There are no conflicts to declare.

Acknowledgements

References

1 B. Sakintuna, F. Lamari-Darkrim and M. Hirscher, *Int. J. Hydrogen Energy*, 2007, **32**, 1121–1140.

2 C. Zhou, Z. Fang, C. Ren, J. Li and J. Lu, *J. Phys. Chem. C*, 2015, **117**, 12973–12980.

3 H. Zijlstra and F. F. Westendorp, *Solid State Commun.*, 1969, **7**, 857–859.

4 J. J. Reilly and R. H. Wiswall, *Inorg. Chem.*, 1968, **7**, 2254–2256.

5 A. Züttel, *Mater. Today*, 2003, **6**(9), 24–33.

6 ENERGY.GOV online, https://energy.gov/eere/fuelcells, accessed on June 10, 2017.

7 A. San-Martin and F. D. Manchester, *Bull. Alloy Phase Diagrams*, 1987, **8**, 431–437.

8 V. Bérubé, G. Radtke, M. Dresselhaus and G. Chen, *Int. J. Energy Res.*, 2007, **31**, 637–663.

9 L. Schlapbach and A. Zuttel, *Nature*, 2001, **414**, 353–358.

10 J. P. Bastide, B. Bonnetot, J. M. Létoffé and P. Claudy, *Mater. Res. Bull.*, 1980, **15**, 1779–1787.

11 P. Vajeeston, P. Ravindran, B. C. Hauback, H. Fjellvåg, A. Kjekshus, S. Furuseth and M. Hanfland, *Phys. Rev. B*, 2006, **73**, 224102.

12 S. Zhou, Q. Zhang, H. Chen, X. Zang, X. Zhou, R. Wang, X. Jiang, B. Yang and R. Jiang, *Int. J. Hydrogen Energy*, 2015, **40**, 11484–11490.

13 J. F. Stampfer Jr, C. E. Holley Jr and J. F. Suttle, *J. Am. Chem. Soc.*, 2002, **82**, 3504–3508.

14 J. C. Crivello, B. Dam, R. V. Denys, M. Dornheim, D. M. Grant, J. Huot, T. R. Jensen, P. de Jongh, M. Latroche, C. Milanese, D. Milčius, G. S. Walker, C. J. Webb, C. Zlotea and V. A. Yartys, *Appl. Phys. A*, 2016, **122**(2), 1–20.

15 C. Suryanarayana, *Prog. Mater. Sci.*, 2004, **46**, 1–184.

16 A. Baldi and B. Dam, *J. Mater. Chem.*, 2011, **21**, 4021–4026.

17 C. E. Buckley, H. K. Birnbaum, J. S. Lin, S. Spooner, D. Bellmann, P. Staron, T. J. Udovic and E. Hollar, *J. Appl. Crystallogr.*, 2001, **34**, 119–129.

18 H. Shao, G. Xin, J. Zheng, X. Li and E. Akiba, *Nano Energy*, 2012, **1**, 590–601.

19 Y. Zhang, S. Liu, T. Yang, G. Zhang, X. Li and D. Zhao, *Rare Met.*, 2014, **34**, 1–9.

20 V. M. Skripnyuk, E. Rabkin, Y. Estrin and R. Lapovok, *Acta Mater.*, 2004, **52**, 405–414.

21 G. Cao, *Nanostructures and Nanomaterials*, World Scientific, New Jersey, 2004.

22 I. Haas and A. Gedanken, *Chem. Commun.*, 2008, **15**, 1795–1797.

23 I. P. Jain, C. Lal and A. Jain, *Int. J. Hydrogen Energy*, 2010, **35**(10), 5133–5144.

24 J. Huot, E. Akiba and T. Takada, *J. Alloys Compd.*, 1995, **231**, 815–819.

25 J. Huot, G. Liang, S. Boily, A. V. Neste and R. Schulz, *J. Alloys Compd.*, 1999, **293–295**(51), 495–500.

26 C. Suryanarayana, E. Ivanov and V. V. Boldyrev, *Mater. Sci. Eng., A*, 2001, **304**, 151–158.

27 R. A. Varin, T. Czujko and Z. S. Wronski, *Nanomaterials for Solid State Hydrogen Storage*, Springer US, New York, 2009.

28 M. Dornheim, *Tailoring Reaction Enthalpies of Hydrides[M]*, Wiley-VCH Verlag GmbH & Co. KGaA, 2010.

29 J. J. Reilly and R. H. Wiswall, *Inorg. Chem.*, 1968, **7**, 2254–2256.

30 M. Pozzo and D. Alfè, *Phys. Rev. B*, 2008, **77**, 104103.

31 X. Hou, H. Kou, T. Zhang, R. Hu, J. Li and X. Xue, *Mater. Sci. Forum*, 2013, **744**, 44–52.

32 N. Terashita, K. Kobayashi, T. Sasai and E. Akiba, *J. Alloys Compd.*, 2001, **327**, 275–280.

33 J. J. Reilly and R. H. Wiswall, *Inorg. Chem.*, 1968, **7**, 2254–2256.

34 H. Shao, G. Xin, X. Li and E. Akiba, *J. Nanomater.*, 2013, **6**, 2527–2531.

35 M. Klell, *Storage of Hydrogen in the Pure Form M*, Wiley-VCH Verlag GmbH & Co. KGaA, 2010.

36 K. Batalović, J. Radaković, J. Belošević-čavor and V. Koteski, *Phys. Chem. Chem. Phys.*, 2014, **16**, 12356–12361.

37 Y. Wang, T. Aizawa and C. Nishimura, *Mater. Trans.*, 2006, **47**, 1052–1057.

38 M. Polanski, T. K. Nielsen, Y. Cerenius, J. Bystrzycki and T. R. Jensen, *Int. J. Hydrogen Energy*, 2010, **35**, 3578–3582.

39 J. Zhang, F. Cuevas, W. Zaïdi, J. P. Bonnet, L. Aymard, J. L. Bobet and M. Latroche, *J. Phys. Chem. C*, 2016, **115**, 4971–4979.

40 D. L. Douglass, *Hydrides for Energy Storage*, 1978, pp. 151–184.

41 G. Liang and R. Schulz, *J. Mater. Sci.*, 2004, **39**, 1557–1562.

42 V. M. Skripnyuk and E. Rabkin, *Int. J. Hydrogen Energy*, 2012, **37**, 10724–10732.

43 B. Thaddeus, *Binary Phase Alloy Diagrams*, Materials Park Ohio, 1990, pp. 2705–2708.

44 H. Zhong, H. Wang, J. Liu, D. Sun and M. Zhu, *Scr. Mater.*, 2011, **65**, 285–287.

45 H. Wang, H. Zhong, L. Ouyang, J. Liu, D. Sun, Q. Zhang and M. Zhu, *J. Phys. Chem. C*, 2014, **118**, 12087–12096.

46 F. Luo, H. Wang, L. Ouyang, M. Zeng, J. Liu and M. Zhu, *Int. J. Hydrogen Energy*, 2013, **38**, 10912–10918.

47 Y. Lu, H. Wang, L. Ouyang, J. Liu and M. Zhu, *J. Alloys Compd.*, 2015, **645**, S103–S106.

48 P. R. Sajanlal, T. S. Sreeprasad, A. K. Samal and T. Pradeep, *Nano Rev.*, 2011, **2**, 1–62.

49 K.-F. Aguey-Zinsou and J.-R. Ares-Fernandez, *Energy Environ. Sci.*, 2010, **3**, 526–543.

50 R. W. Wagemans, J. H. van Lenthe, P. E. de Jongh, A. J. van Dillen and K. P. de Jong, *J. Am. Chem. Soc.*, 2005, **127**, 16675–16680.

51 W. Liu and K. F. Agueyzinsou, *J. Mater. Chem. A*, 2014, **2**, 9718–9726.

52 J. Lu, Y. J. Choi, Z. Fang and H. Y. Sohn, *J. Am. Chem. Soc.*, 2009, **131**, 15843–15852.

53 K. Asano, R. J. Westerwaal, A. Anastasopol, L. P. A. Mooij, C. Boelsma, P. Ngene, H. Schreuders, S. W. H. Eijt and B. Dam, *J. Phys. Chem. C*, 2015, **119**, 12157–12164.

54 S. Bouaricha, J. P. Dodelet, D. Guay, J. Huot and R. Schulz, *J. Mater. Res.*, 2001, **16**, 2893–2905.

55 S. Zhou, X. Zhang, T. Li, N. Wang, H. Chen, T. Zhang, H. Yu, H. Niu and D. Liu, *Int. J. Hydrogen Energy*, 2014, **39**, 13628–13633.

56 M. Calizzi, F. Venturi, M. Ponthieu, F. Cuevas, V. Morandi, T. Perkisas, S. Bals and L. Pasquini, *Phys. Chem. Chem. Phys.*, 2016, **18**, 141–148.

57 J. A. Puszkiel, P. A. Larochette and F. C. Gennari, *J. Power Sources*, 2009, **186**, 185–193.

58 K. J. Gross, P. Spatz, A. Zuettel and L. Schlapbach, *J. Alloys Compd.*, 1996, **27**, 206–213.

59 W. Li, C. Li, H. Ma and J. Chen, *J. Am. Chem. Soc.*, 2007, **129**, 16675–16680.

60 L. Li, B. Peng, W. Ji and J. Chen, *J. Phys. Chem. C*, 2009, **113**, 3007–3013.

61 H. Fujii, K. Higuchi, K. Yamamoto, H. Kajioka, S. Orimo and K. Toiyama, *Mater. Trans.*, 2002, **43**, 2721–2727.

62 K. Higuchi, K. Yamamoto, H. Kajioka, K. Toiyama, M. Honda, S. Orimo and H. Fujii, *J. Alloys Compd.*, 2002, **330**, 526–530.

63 H. Wang, L. Ouyang, C. Peng, M. Zeng, C. Chung and M. Zhu, *J. Alloys Compd.*, 2004, **370**, L4–L6.

64 S. Singh, S. W. H. Eijt, M. W. Zandbergen, W. J. Legerstee and V. L. Svetchnikov, *J. Alloys Compd.*, 2007, **441**, 344–351.

65 W. P. Kalisvaart, C. T. Harrower, J. Haagsma, B. Zahiri, E. J. Luber, C. Ophus, E. Poirier, H. Fritzsche and D. Mitlin, *Int. J. Hydrogen Energy*, 2010, **35**, 2091–2103.

66 B. Zahiri, M. Danaie, X. Tan, S. Amirkhiz, G. A. Botton and D. Mitlin, *J. Phys. Chem. C*, 2011, **116**, 3188–3199.

67 A. Baldi, M. Gonzalez-Silveira, V. Palmisano, B. Dam and R. Griessen, *Phys. Rev. Lett.*, 2009, **102**, 226102.

68 C. J. Chung, S. C. Lee, J. R. Groves, E. N. Brower, R. Sinclair and B. M. Clemens, *Phys. Rev. Lett.*, 2012, **108**, 106102.

69 L. P. A. Mooij, A. Baldi, C. Boelsma, K. Shen, M. Wagemaker, Y. Pivak, H. Schreuders, R. Griessen and B. Dam, *Adv. Energy Mater.*, 2011, **1**, 754–758.

70 J. R. H. Luke, *Hydrogen sorption properties of magnesium-based thin films*, University of Birmingham, 2016.

71 S. Zhang, A. F. Gross, S. L. Van Atta, M. Lopez, P. Liu, C. C. Ahn, J. J. Vajo and C. M. Jensen, *Nanotechnology*, 2009, **20**, 204027.

72 Y. Liu, J. Zou, X. Zeng, X. Wu, H. Tian, W. Ding, J. Wang and A. Walter, *Int. J. Hydrogen Energy*, 2013, **38**, 5302–5308.

73 Y. S. Au, M. K. Obbink, S. Srinivasan, P. C. M. M. Magusin, K. P. De Jong and P. E. de Jongh, *Adv. Funct. Mater.*, 2014, **24**, 3604–3611.

74 Y. Jia, C. Sun, L. Cheng, W. M. Abdul, J. Cui, J. Zou, M. Zhu and X. Yao, *Phys. Chem. Chem. Phys.*, 2013, **15**, 5814–5820.

75 K. J. Jeon, H. R. Moon, A. M. Ruminski, B. Jiang, C. Kisielowski, R. Bardhan and J. J. Urban, *Nat. Mater.*, 2011, **10**, 286–290.

76 H. Li, Z. Song, X. Zhang, Y. Huang, S. Li, Y. Mao, H. Ploehn, Y. Bao and M. Yu, *Science*, 2013, **342**, 95–98.

77 H. Jung, S. Yang, T. Kim, J. Kang and R. Chong, *Carbon*, 2013, **63**, 165–174.

78 E. S. Cho, A. M. Ruminski, Y. Liu, P. T. Shea, S. Kang, E. W. Zaia, J. Y. Park, Y. D. Chuang, J. M. Yuk, X. Zhou, T. W. Heo, J. Guo, B. C. Wood and J. J. Urban, *Adv. Funct. Mater.*, 2017, **27**, 1704316.

79 J. Cui, H. Wang, D. Sun, Q. Zhang and M. Zhu, *Rare Met.*, 2016, **35**, 401–407.

80 M. Paskevicius, D. A. Sheppard and C. E. Buckley, *J. Am. Chem. Soc.*, 2010, **132**, 5077–5083.

81 M. Bortz, B. Bertheville, G. Böttger and K. Yvon, *J. Alloys Compd.*, 1999, **287**(3), 4–6.

82 J. Huot, G. Liang, S. Boily, A. V. Neste and R. Schulz, *J. Alloys Compd.*, 1999, **293–295**, 495–500.

83 X. Xiao, Z. Liu, S. Saremiyarahmadi and D. H. Gregory, *Phys. Chem. Chem. Phys.*, 2016, **18**, 10492–10498.

84 C. Ren, Z. Fang, C. Zhou, J. Lu, Y. Ren, X. Zhang and X. Luo, *Int. J. Hydrogen Energy*, 2014, **39**, 5868–5873.

85 C. Shen and K. F. Aguey-Zinsou, *J. Mater. Chem. A*, 2017, **5**, 8644–8652.

86 M. Ponthieu, F. Cuevas, J. F. Fernández, L. Laversenne, F. Porcher and M. Latroche, *J. Phys. Chem. C*, 2013, **117**, 18851–18862.

87 F. C. Gennari, F. J. Castro and G. Urretavizcaya, *J. Alloys Compd.*, 2001, **321**, 46–53.

88 Y. Song and Z. Guo, *Appl. Phys. Lett.*, 2006, **89**, 151.

89 J. J. Vajo, T. T. Salguero, A. F. Gross, S. L. Skeith and G. L. Olson, *J. Alloys Compd.*, 2007, **446**(1), 409–414.

90 J. J. Vajo, F. Mertens, C. C. Ahn, R. C. Bowman and B. Fultz, *Cheminform*, 2004, **35**, 13977–13983.

91 A. L. Chaudhary, D. A. Sheppard, M. Paskevicius, C. J. Webb, E. M. Gray and C. E. Buckley, *J. Phys. Chem. C*, 2013, **118**, 1240–1247.

92 S. T. Kelly, S. L. Van Atta, J. J. Vajo, G. L. Olson and B. M. Clemens, *Nanotechnology*, 2009, **20**, 204017.

93 F. C. Gennari, F. J. Castro, G. Urretavizcaya and G. Meyer, *J. Alloys Compd.*, 2002, **334**, 277–284.

94 G. S. Walker, M. Abbas, D. M. Grant and C. Udeh, *Chem. Commun.*, 2011, **47**, 8001–8003.

95 S. Bouaricha, J. P. Dodelet, D. Guay, J. Huot, S. Boily and R. Schulz, *J. Alloys Compd.*, 2000, **297**, 282–293.

96 J. C. Crivello, T. Nobuki and T. Kuji, *Int. J. Hydrogen Energy*, 2009, **34**, 1937–1943.

97 S. Kalinichenka, L. Röntzsch, T. Riedl, T. Weißgärber and B. Kieback, *Int. J. Hydrogen Energy*, 2011, **36**, 10808–10815.

98 H. Lin, W. Wang and M. Zhu, *J. Non-Cryst. Solids*, 2012, **358**, 1387–1390.

99 A. Ming, *Mater. Sci. Eng., B*, 2005, **117**, 37–44.

100 N. Zhou and D. Ju, *Int. J. Hydrogen Energy*, 2014, **39**, 19630–19636.

101 S. Kumar, U. Jain, A. Jain, H. Miyaoka, T. Ichikawa, Y. Kojima and G. K. Dey, *Int. J. Hydrogen Energy*, 2017, **47**, 3963–3970.

102 S. V. Alapati, J. J. Karl and D. S. Sholl, *Phys. Chem. Chem. Phys.*, 2007, **38**, 1438–1452.

103 J. J. Vajo, W. Li and P. Liu, *Chem. Commun.*, 2010, **46**, 6687–6689.

104 H. Liu, X. Wang, Y. Liu, Z. Dong, H. Ge, S. Li and M. Yan, *J. Phys. Chem. C*, 2014, **118**, 37–45.

105 M. Jurczyk, M. Nowak, L. Smardz and A. Szajek, *Mg-BASED NANOCOMPOSITES FOR ROOM TEMPERATURE HYDROGEN STORAGE*, Tms 1 Meeting & Exhibition, 2011.

106 L. E. Klebanoff and J. O. Keller, *Int. J. Hydrogen Energy*, 2013, **38**, 4533–4576.

107 Y. Liu, K. Zhong, M. Gao, J. Wang, H. Pan and Q. Wang, *Chem. Mater.*, 2008, **20**, 3521–3527.

108 J. J. Hu, E. Rohm and M. Fichtner, *Acta Mater.*, 2011, **59**, 5821–5831.

109 J. Lu, Y. J. Choi, Z. Z. Fang and Y. Hong, *J. Power Sources*, 2010, **195**, 1992–1997.

110 J. Lu, Z. Z. Fang, Y. J. Choi and H. Y. Sohn, *MRS Online Proc. Libr.*, 2007, **111**, 12129–12134.

111 O. Dolotko, N. Paulson and V. K. Pecharsky, *Int. J. Hydrogen Energy*, 2010, **35**, 4562–4568.

112 R. Parviz and R. A. Varin, *Int. J. Hydrogen Energy*, 2013, **38**, 8313–8327.

113 R. A. Varin, R. Parviz, M. Polanski and Z. S. Wronski, *Int. J. Hydrogen Energy*, 2014, **39**, 10585–10599.

114 G. Xia, X. Chen, C. Zhou, C. Zhang, D. Li, Q. Gu, Z. Guo, H. Liu, Z. Liu and X. Yu, *J. Mater. Chem. A*, 2015, **3**, 12646–12652.

115 B. Zhang and Y. Wu, *Prog. Nat. Sci.: Mater. Int.*, 2017, **27**(1), 21–33.

116 A. Zaluska, L. Zaluski and J. O. Ström-Olsen, *J. Alloys Compd.*, 1999, **289**, 197–206.

117 Z. Li, X. Liu, L. Jiang and S. Wang, *Int. J. Hydrogen Energy*, 2007, **32**, 1869–1874.

118 L. Laversenne, J. Andrieux, D. Plante, L. Lyard and S. Miraglia, *Int. J. Hydrogen Energy*, 2013, **38**, 11937–11945.

119 X. Liu, Z. Huang, L. Jiang and S. Wang, *Int. J. Hydrogen Energy*, 2007, **32**, 965–968.

120 C. Zhou, Z. Z. Fang, C. Ren, J. Li and J. Lu, *J. Phys. Chem. C*, 2013, **117**, 12973–12980.

121 F. Li, L. Jiang, J. Du, S. Wang, X. Liu and F. Zhan, *Int. J. Hydrogen Energy*, 2006, **31**, 581–585.

122 G. Liang, S. Boily, J. Huot, A. V. Neste and R. Schulz, *J. Alloys Compd.*, 1998, **268**, 302–307.

123 G. Liu, Y. Wang, L. Jiao and H. Yuan, *Int. J. Hydrogen Energy*, 2014, **39**, 3822–3829.

124 D. W. Lim, J. W. Yoon, K. Y. Ryu and M. P. Suh, *Angew. Chem.*, 2012, **51**, 9814–9817.

125 B. P. D. Ulf, E. P. D. Baldur and G. Taylor, *Cogeneration and Competitive Power Journal*, 2003, **18**(3), 29–70.

126 X. B. Yu, Z. W. Tang, D. L. Sun, L. Z. Ouyang and M. Zhu, *Prog. Mater. Sci.*, 2017, **88**, 1–48.

127 I. Z. Hlova, *Mechanochemical synthesis of hydrogen-storage materials based on aluminum, magnesium and their compounds*, Iowa State University, 2015.